COMPARISON OF ELECTRICITY PRODUCTION BETWEEN SEMI-SUBMERSIBLE AND SPAR-BUOY FLOATING OFFSHORE WIND TURBINES

Dissertation in partial fulfillment of the requirements for the degree of

MASTER OF SCIENCE
WITH A MAJOR IN WIND POWER PROJECT MANAGEMENT

UPPSALA
UNIVERSITET

Uppsala University
Department of Earth Sciences, Campus Gotland

Nermina Saračević

24 September 2018

COMPARISON OF ELECTRICITY PRODUCTION BETWEEN SEMI-SUBMERSIBLE AND SPAR-BUOY FLOATING OFFSHORE WIND TURBINES

Dissertation in partial fulfillment of the requirements for the degree of

MASTER OF SCIENCE
WITH A MAJOR IN WIND POWER PROJECT MANAGEMENT

Uppsala University
Department of Earth Sciences, Campus Gotland

Approved by:

Supervisor,	Dr. Hugo Espinosa Olivares, Uppsala University
Co-supervisor,	Anders Wickström, Scandinavian Wind AB
Examiner,	Prof. Dr. Jens Nørkær Sørensen, Danish Technical University

24 September 2018

ABSTRACT

The paper compares electricity production between the semi-submersible and the spar-buoy floating wind turbine systems under normal, stochastic and extreme wind conditions at Utsira Nord site located on the Norwegian continental shelf in the North Sea. The analysis of complex behavior of the floating wind turbine system and the fluid-structure interaction is performed in aero-servo-hydro-elastic code ASHES.

The results indicate a slightly better energy performance of the semi-submersible than the spar in all load cases but one. The pitch and heave degrees of freedom are evaluated as the most relevant for the power output. It is shown that pitch and heave platform motions have smaller displacement in the semi-submersible floater than in the spar under average environmental conditions and at the rated wind speed operating range. The simulation also confirmed that the energy yield is very sensitive to the magnitude of the loads: the spar performed best under mild environmental conditions, while the semi-submersible was better under medium environmental conditions. Small difference in energy yield is attributed to the same baseline blade and external controller properties used for both floaters where generator torque was kept constant to limit the power excursions above the rated power.

The method proposed under this paper has demonstrated that a good approximation of the energy performance of the floating wind turbine system can be performed in a fast and effective manner.

Key words: *floating offshore wind turbine, semi-submersible, spar-buoy, six degrees of freedom, platform-rotor interaction, ASHES*

ACKNOWLEDGEMENTS

I wish to extend a tremendous gratitude to my academic supervisor Dr. Hugo Espinosa Olivares for his genuine support, great eye for detail and the constructive direction in the preparation of this thesis. I have greatly benefited from his research zeal and the ability to clarify complex issues with the precision and simplicity.

I would also like to express my appreciation to Anders Wickström, from Scandinavian Wind AB, who kindly consented to support my work as a co-supervisor from the wind industry. His suggestions were highly insightful, practical and valuable in regards to selection of the topic and the modeling tool.

Furthermore, my enormous gratitude goes to Paul Thomassen and Loup Suja from SIMIS AS, for allowing me to use ASHES in my analysis and for being extremely patient and supportive in answering all my questions. Even though this was during the summer break.

Special thanks goes to my colleague Bojan Alavanja for his continuous encouragement and assistance throughout this Master program.

I am very much grateful to Uppsala University for supporting my academic endeavors by awarding me the IPK scholarship and distinguishing me with the Global Swede 2018 Award.

Finally, I wish to thank to my family for always being there where it exactly should be.

NOMENCLATURE

AEP	Annual Energy Production
BEM	Blade Element Momentum
CFD	Computational Fluid Dynamics
DNV	Det Norske Veritas
DLL	Dynamic Link Library
DoF	Degree of Freedom
ETM	Extreme Turbulence Model
EWM	Extreme Wind Speed
FAST	Fatigue, Aerodynamics, Structures & Turbulence
FEM	Finite Element Momentum
FOWT	Floating Offshore Wind Turbine
IEC	International Electrotechnical Commission
NREL	National Renewable Energy Laboratory
NTM	Normal Turbulence Model
OpenFOAM	Open-source Field Operation and Manipulation
RNA	Rotor Nacelle Assembly
RPM	Revolutions Per Minute
SSL	Standard Sea Level
SWL	Sea Water Level
TLP	Tension Leg Platform
TSR	Tip Speed Ratio
WTG	Wind Turbine Generator

TABLE OF CONTENTS

LIST OF FIGURES

LIST OF TABLES

Chapter 1

Introduction

1.1 Motivation and objective of the research

From the perspective of the wind industry, the floating offshore wind in deep waters represents a major unlocked potential for the future electricity supply. European Wind Energy Agency (EWEA) has identified already in 2013 that there were approximately 4000 GW of the floating wind potential in the European Seas in deep waters (>60 m), the majority of which is located in the North Sea (Wind Europe, 2017). But before a full scale commercialization is possible, there should be an advanced understanding of the technology performance based on accurate energy predictions. The present research aims to provide a practical insight into a modeling approach for comparison of energy output of floaters in the initial phase of a floating offshore wind farm development.

1.2 Research question

Which type of the floating offshore concept, spar or semi-submersible, has a superior performance in terms of energy yield under steady, stochastic and extreme wind conditions on the Norwegian continental shelf in the North Sea?

1.3 Hypothesis

Due to smaller platform motion of the semi-submersible floater in heave and pitch modes, there is less impact on the hub displacements which gives better electricity output as compared to the spar-buoy floater.

1.4 Methodology

Under the limited scope of the current work, it was decided to use a novel aero-hydro-elastic code with improved visualization effects called “ASHES” to model and simulate 6 load cases for both types of floaters. This method represents modeling compromise because floating wind turbine analysis usually requires combination of two or more codes to model its complex system features. However, we believe that the most prominent aspects are being addressed and that the resulting estimate of power is a good indication of what happens in reality.

1.5 Limitations

This paper will not provide in-depth analysis of the coupled fluid-structure interaction of the floating wind turbines, because ASHES cannot simultaneously capture full aerodynamic effects of unsteady flow around the rotor. Another limiting factor is that only one turbine can be simulated at the time, which excludes analysis of entire wind park and the associated wake effects from turbines placed in array. Only spar and semi-submersible floaters will be evaluated because the last version of ASHES (3.3.1) used in this research did not support modeling of tension leg platform floater. The current analysis will focus on the impact of platform motion on nacelle and will not investigate the influence of rotor control mechanism on platform motion which may constitute a separate analysis.

1.6 Outline of the paper

After a brief overview of the thesis structure in the current chapter, the chapter 2 will present literature review on the floating turbine technology, its design and main modeling challenges. Chapter 3 will outline a methodology approach used in modeling different components of the floating wind turbines and introduce load cases. Chapter 4 will present a case study, describe how the methodology will be applied and define input data. The main findings will be discussed in chapter 5, while chapter 6 will summarize conclusions and give recommendations for further research.

Chapter 2

Review of FOWT design challenges

This chapter will present literature review of the most prominent issues concerning development of the floating wind turbine technology, including the environmental and load conditions, design issues and modeling techniques.

2.1 Why investing in floating offshore wind technology?

The energy demand will undoubtedly increase in the future due to population growth, economic and trade integrations, improvement of life standard and technological advancements. In order to meet this demand in a sustainable manner, European Commission has set out an ambitious agenda in its Energy Roadmap 2050 to decrease the greenhouse gas emissions by 80-95% below 1990-level by 2050. Among other measures, the Roadmap called for a transition to the low carbon economy by deploying high level of renewable energy sources (RES), targeting gross final energy consumption of 75% and electricity consumption 97% from RES by 2050[1] (European Commission, 2011). Such a High RES Scenario should be realized by increased use of hydro, wind, solar, biomass, wave and geothermal resources. In particular, wind is expected to be the

[1] The Energy Roadmap 2050 is part of EU energy *acquis* and as such it is a binding legislation for the EU member states. The Roadmap provides guidance to individual energy policies of other European countries which are not part of the EU, but are either joining EU (accession countries) or are members of the European Economic Area. In this context, the Energy Roadmap sets out a general policy framework for de-carbonization strategy across entire European continent.

primary renewable source for generating electricity in Europe in 2050 and more specifically, the offshore wind resources in North and Atlantic Seas (European Commission, 2011).

The share of wind power installation has risen significantly since 2005 in EU: from 40.7 GW in 2005 to 168.7 GW of cumulative installed capacity for onshore and offshore wind in 2017. In the same year, the wind power was the fastest growing source of newly installed power generating capacity in Europe, being a champion among RES and supplying 11.7% of the European electricity demand (Wind Europe, 2017). In the recent years, the onshore wind installation in Europe is slowly approaching a saturation point moving to the offshore sites where wind farms are installed with the bottom-fixed technology. This is mainly due to the absence of large scale visual and noise impact that is often a constraint to onshore wind parks. Secondly, further from the shore the wind is stronger and more constant, and possibility to install bigger rotor means capturing more kinetic energy to balance off the investment costs.

Currently, the fixed bottom offshore wind farms are mainly located closer to the shore (up to 30 km) and in the shallow waters up to 50-60 m. The offshore wind turbines are fixed to the seabed by bottom mounted foundations of monopole or jacket (tripod) type. However, there are significant structural and economic limitations when it comes to applying the bottom-mounted foundations in the water deeper than 50 m. The drilling and installation of the foundations into the seabed at higher water depth would be technically limited involving complex logistics that would increase CAPEX[2]. The decommissioning of bottom fixed structures is already a challenging issue for the shallow waters raising environmental concerns and would be even bigger problem in the deeper waters (Carbon Trust, 2015). This limits potential for wind exploitation to many countries that have deep waters along their coast, such as Portugal, Norway, Japan, US.

Contrary to the seabed fixed foundations, the installation of the floating wind turbines could be faster allowing the assembly and commissioning of wind turbines onshore,

[2] Capital expenses.

transfer to the offshore site and less complex installation using specific anchoring and mooring systems. Such a design would enable installation of future offshore wind farms to up to 200 km from the shore in an average water depth of 215 m (EWEA, 2013).

The industrial research has demonstrated that the floating offshore concept can build upon the experience of the bottom-fixed foundations and floating platforms used by oil and gas industry. Carbon Trust report (2015) reviewed 18 different concepts out of more than 30, in order to assess technological and market trends of the floating offshore wind. Their conclusion indicated that a good potential exists for this technology to get mature over the next couple of years and that the Levelized Cost of Energy (LCOE)[3] can decrease to £85-100 MWh depending on the level of advancement of a prototype (Carbon Trust, 2015).

With the world's first floating wind farm Hywind (spar buoy) installed by Norwegian Statoil (today Equinor) in 2017 near the Scottish coast, the technology seems to be on the verge of break-through for a commercial deployment in the next 5 years. The European front-runners in research and development are Norway, Portugal and France. Norwegian government recently announced plans to unveil two new test sites along its coast by the end of 2018. France has in pipeline a couple of pilot projects for 2020 that would be based on semi-submersible design (Naval Energies): Maine Acqua Ventus (12 MW) and French Groix-Belle-Île (24 MW). Another project - WindFloatAtlantic is expected to be launched next year by Portugal (Deign, 2018). All these projects are expected to contribute to a full-scale deployment of the floating wind technology and ultimately, to generation of clean electricity in Europe.

2.2 Characteristics and typology of FOWT

The floating offshore wind turbine system is the most complex one of all wind power concepts. It consists of multiple components: horizontal-axis turbine (although vertical-axis are also used in some prototypes), a tower, a buoyant platform (floater), moorings

[3] LCOE is a net present value of the unit cost of electricity produced over a lifetime of a wind farm. It is the minimum amount of revenue needed to cover all costs for investment and operation of a wind farm.

and anchoring system. The term "floating station" will be used here interchangeably with the "floating structure" or "floating system" to denote its composite configuration.

FOWT system is distinguished based on the type of the floater (or floating platform) chosen to support the Rotor-Nacelle-Assembly (RNA). Three major platform concepts have evolved over the last three decades of intensive research: spar-buoy[4] (stabilized by ballast), semi-submersible[5] (stabilized by buoyancy from large floating hull) and tension leg platform – TLP (stabilized by the mooring system), as illustrated in Figure 1. There can be many different variations within these 3 main categories depending on the site conditions, mooring lines, tanks and ballast. Besides that, novel concepts include multi-turbine (semi-submersible platform carrying multiple rotors) and hybrid designs which are combination of wind turbine rotors and the wave or tidal energy devices (Carbon Trust, 2015).

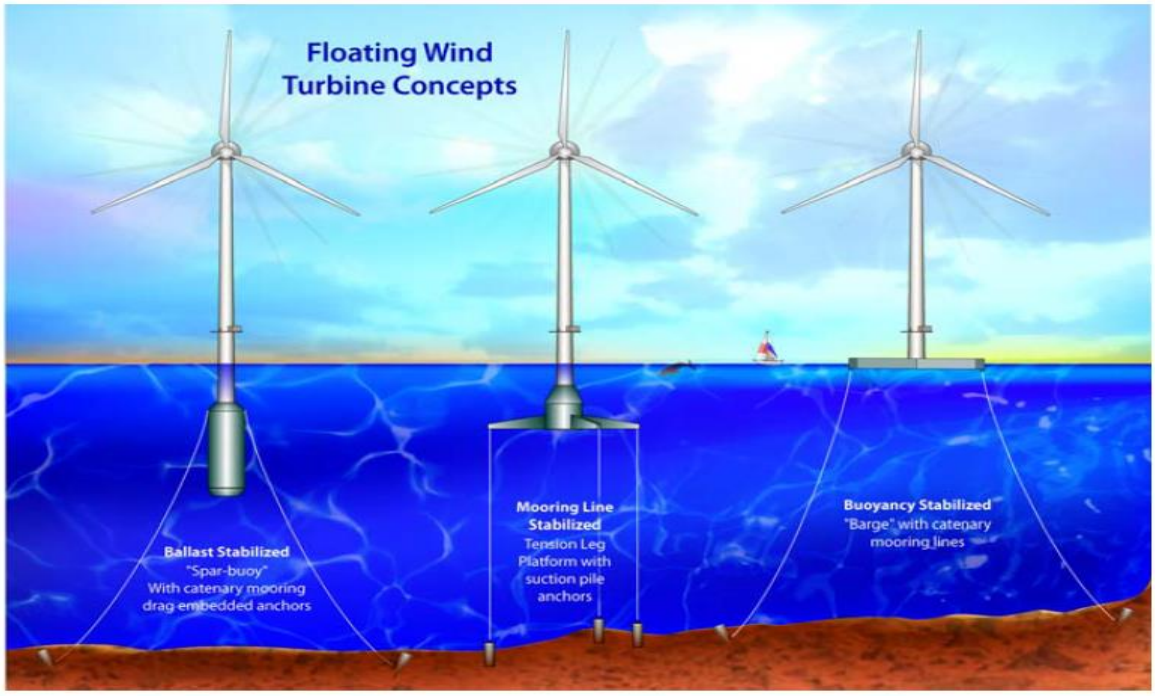

Figure 1: Three main prototypes of FOWT (Butterfield et al., 2005)

[4] Also referred as Spar.

[5] Semi-submersible typology includes also Barge floaters.

2.2.1 Spar-buoy

This type consists of a long vertical cylinder (draft) which is submerged in the water and usually anchored by three catenary moorings. On its lower end and closer to the ground there is a ballast for stability, which makes this part heavier, while the upper part closer to the water surface is lighter (empty). In this way, centre of gravity (mass) is lower in the water and counterbalanced by the centre of buoyancy (closer to the surface) enabling the structure to float. The *Hywind* is considered to be so far the most advanced prototype, developed by Norwegian oil and gas company Statoil and tested for the first time with 2.3 MW turbine in 2009 near the Norwegian shore. A follow-up design has aimed to improve overall mass and replace water with stone ballast (Carbon Trust, 2015). In 2017, Statoil has installed a first world's floating wind farm, *Hywind* which has 30 MW capacity, comprised of 5x6MW Siemens turbines (Equinor, 2018).

2.2.2 Tension leg platform (TLP)

This concept is based on the anchoring the semi-submerged structure by tensioned mooring lines (tendons). The rather small and light buoyant structure is drifting little bit below the surface of water. Since the floating structure is lighter, there is more stress (or tension) on the mooring lines to support stability. The *Blue H TLP* prototype is based on a submerged buoyant structure which is tightly linked to the seabed by 3 tensioned moorings to ensure uplifting force. The platform is rigidly fixed through moorings attached to three gravity anchors, which can fit into any type of the seabed. This prototype was first installed in 2008 along Italian cost and recent upgrade is aimed to decrease the structural weights (Carbon Trust, 2015).

2.2.3 Semi-submersible

This configuration consists of a larger buoyant structure that is semi-submerged and anchored to seabed by the catenary moorings. The floating structure is made of three or four columns interconnected by steel bars (Liu et al., 2016). The submerged structure needs to have big plane area heavy enough to achieve the necessary stability.

The *WindFloat* semi-submersible is the second most famous concept after *Hywind*'s spar. It was designed by Principle Power and installed in 2011 close to Portuguese shore. This design includes a semi-submerged hull which consists of three interconnected columns and horizontal axis turbine which is mounted on one of these columns. The floating platform has water ballast and heave (entrapment) plates on the base of each column, to dampen platform motion and provide stability. This configuration has high commercial potential due to its stable performance and it is considered that it can accommodate almost any modern turbine (Carbon Trust, 2015).

2.3 Environmental conditions

Operation of the floating turbine is affected by different environmental loads that include meteorological and ocean phenomena (met-ocean conditions), soil conditions, seismicity, local ecosystem. Combination of all these factors represent local climate in which FOWT should operate over the next 20-25 years. Specifications of environmental conditions and design loads that are applicable to FOWT are described in the Det Norske Veritas standard - DNV OS-J103 (2013) as well as in the International Electro-technical Commission - IEC 61400-3 (2009) standard. Both DNV and IEC standards provide overview of technical requirements for design, construction and in-service inspection of the FOWT.

The following environmental loads affect operation of the FOWT:

- *Aerodynamic loads* created by air (wind, gusts, turbulence, wakes) and rotor dynamics
- *Hydrodynamic loads* (waves, currents, tide)
- *Other loads* (earthquakes, marine growth and icing, snow)

2.3.1 Wind climate

Wind is horizontal movement of air characterized by certain velocity and direction. Further from the coast, the offshore wind is stronger because there are no obstructions. Turbulence is smaller due to relatively flat sea surface and larger distance from the coast,

followed by low roughness and small wind shear (Barthelmie, 1999 as cited in Türk & Emeis, 2010). In some cases, roughness can be higher because of the strong waves, which can increase turbulence.

Offshore wind profile is usually described by the following parameters (Burton et al., 2011):

- Wind speed and direction
- Turbulence intensity at operating range and at extreme speed
- Standard deviation of turbulence intensity at each wind speed
- Extreme 10 minute mean wind speed with recurrence period of 50 years
- Wind shear
- Air density

Wind shear represents increase in wind speed due to distance in height from the surface to the hub and depends on the sea roughness created by waves. In the sea environment, wind shear is relatively low, because of small roughness length which is around zero (0.0002 m). Another important aspect for wind profile is turbulence, which represents random fluctuation in wind speed and direction followed by gusts. Turbulence intensity is defined under IEC 61400-1 standard as a ratio of wind speed standard deviation to mean wind speed. As mentioned above, the turbulence is smaller because there are no obstacles and secondly, because there is better absorption of the heat by water surface so the differences between air and water temperature is smaller (Danish Wind Industry Association, 2013).

2.3.2 Sea climate

Waves are mainly created by the wind blowing over the water which disturbs its flat surface, creating motion. Less common are tidal waves caused by the gravitational forces of sun and moon. The sea is represented by many small waves that are grouped in the so-called wave or frequency spectra where each sub-group of waves has its own amplitude, direction and frequency.

In the analysis of site specific sea data, the wave climate is represented by the sea states. The sea states are determined by the significant wave height (H_s) and the wave period taken as average of all wave components (T_m). Different sea states are presented as frequency distribution over certain period of time and per wave direction in the format of scatter diagram (Beels et al., 2007). Besides wave conditions, IEC 61400-1 standard prescribes that the sea climate modeling should include currents, defined as steady flow fields with constant velocity and direction that change with the water depth.

2.3.3 Representation of offshore climate

For modeling environmental conditions at offshore sites, DNV OS-J103 guidelines indicate that a proper correlation between wind, wave and currents data should be established as a long term probability distribution, which is usually expressed as 2D or 3D scatter diagrams.

The DNV standard distinguishes between stationary and extreme wind and wave conditions that can be observed from environmental data at a given site. Similarly, IEC 61400-3 standard defines wind regime as either normal (wind conditions occur frequently over a year) and extreme (where wind conditions have 1- or 50- year recurrence period). Same applies for extreme sea state which is defined by the significant wave height that can have recurrence periods of 1 or 50 years. Normal (real) wave climate is represented by the stochastic sea state model as either Pierson-Moskowitz or Jonswap spectrum. The stochastic sea states would include stationary values of the significant wave height, peak spectral period and mean wind speed per each sea state. For analysis of wave loads under specific sea state a deterministic wave model is used.

Consequently, the assessment of environmental conditions that prevail at a specific site should take into account the following parameters according to DNV-OS-J103:

- Significant wave height
- Peak wave period (or zero-upcrossing period)
- Mean wave direction

- Directional spreading of waves
- 10-minute mean wind speed at reference height
- Standard deviation of wind speed
- Mean wind direction
- Misalignment between wind and wave directions
- Currents

As specified under DNV 61400-3 standard, the stationary wind conditions usually include constant 10-minute average wind speed (U_{10}) and constant standard deviation (σ_u) of the mean wind speed. U_{10} represents wind intensity and σ_u how much the wind speed varies around mean wind speed. Stationary wave conditions refer to those values of significant wave height (H_s) and peak spectral period (T_P) that are constant over 3 or 6 hours period. T_p represents the period dominated by the highest energy wave component. However, due to the difference in the averaging period of the wind and wave data, it is necessary to adjust averaging of data by taking wind speed data of at least 1 hour and not 10 minutes, which is normally used as a reference value for onshore sites.

2.4 Design challenges

Due to interplay of different loads that act on the floating structure, designers are faced with the challenge to reduce fatigue and ensure system's stability at a profitable cost. The following issues will be discussed in the next sections as the most relevant for the current analysis: the floater motion, the rotor-floater dynamics and the modeling technique for simulating flow-structure dynamics.

2.5 Floater motion

The movement of supporting platform is influenced by its stiffness, dynamic responses and six degrees of freedom which contribute to acceleration of the rotor hub creating vortices and wakes. These combined properties change amplitude and frequency of the platform motion to a various degree and are important in understanding the floater interaction with the rotor dynamics in the analysis of energy output.

2.5.1 System stiffness

Due to its specific geometry, FOWT displays non-linear dynamic behavior compared to conventional onshore and offshore wind turbines. In particular, hydrostatic and mooring static characteristics of the floater are responsible for non-linear dynamic responses of the floating platform and are critical for ensuring static stability. The stiffness of any structure refers to its ability to sustain given forces and loads before it deforms. In FOWT, the system stiffness refers to hydrostatic stiffness and mooring static stiffness, which have different properties per each floating type. Al-Solihat & Nahon (2015) specify that the hydrostatic stiffness of the floater should sustain hydrostatic restoring forces and moments induced by buoyancy and gravity forces. Mooring stiffness should endure loads relevant to the platform displacements. The authors analyzed the system stiffness calculating and comparing the hydrostatic and mooring stiffness coefficients for three types of FOWT (spar, barge and TLP). Results showed that the slack/catenary mooring system configurations which are typical for spar, semi-submersible and barge depend mostly on large hydrostatic stiffness to ensure system stability compared to taut mooring systems, which rely on large mooring stiffness (TLP floater). The barge/semi-submersible type exhibited bigger hydrostatic heave stiffness than spar due to larger water plane surface (Al-Solihat & Nahon, 2015).

All physical bodies oscillate when exposed to external force at some frequency, which is its natural frequency (eigenfrequency). A body can have many natural frequencies but the most important for wind turbine is the first tower bending frequency that should resonate below the frequency of a certain excitation force. Resonance occurs when the body/structure is excited by an external force to vibrate at higher amplitude within specific frequency (Hau, 2013).

In the floating wind turbines, the structural loads from nacelle (thrust, torque and yaw) can be counteracted by increasing stiffness either through enlarged water plane area (e.g. tri-floater, semi-submerged platform), or by mooring tendons (e.g. TLP) or by stiffness that is obtained from a large mass placed under the water (e.g. spar floater).

However, increasing stiffness of a floating structure to balance the aerodynamic loads may create too large hydrostatic stiffness causing the structure's resonance to be same as the resonance of the wave (Henderson, 2009), which causes high level of vibration. When the structure's first natural bending frequency coincides with the excitation frequency from wind, wave or rotor, the structure can become weak, sensitive to fractures and fatigue, failing to survive long years of operation. One method to reduce resonant oscillations which are caused by hydrodynamic force of the wave is to decrease the directly exposed area of the structure towards the waves either by submerging the floating structure deeper under the water line level or by increasing it above the water line level. This would reduce the effect of the wave resonance on the natural vibration frequency of the floating structure. Other methods may be also effective such as increasing the damping by adding the active damping devices (heave plates) at the bottom of platform (Henderson, 2009). Adding the heave plates would increase mass of the structure, suppress vortices and adjust natural frequency of the floating structure (Longbin & Shunqing, 2004).

2.5.2 The six degrees of freedom

The flow field around the floating turbine is influenced by what is known as "6 degrees of freedom of the platform movement". That involves 3 translational components (heave in vertical, sway in lateral and surge in axial direction), which are distributed along x, y, z spatial coordinates with origin point at the center of gravity of the platform. Another three rotational components (yaw motion around vertical axis, pitch along lateral, and roll around axial direction) are moving along the $x^{'}$, $y^{'}$, $z^{'}$ coordinates, which are aligned with the hub rotational plane (Tran & Kim, 2015) as shown in Figure 2.

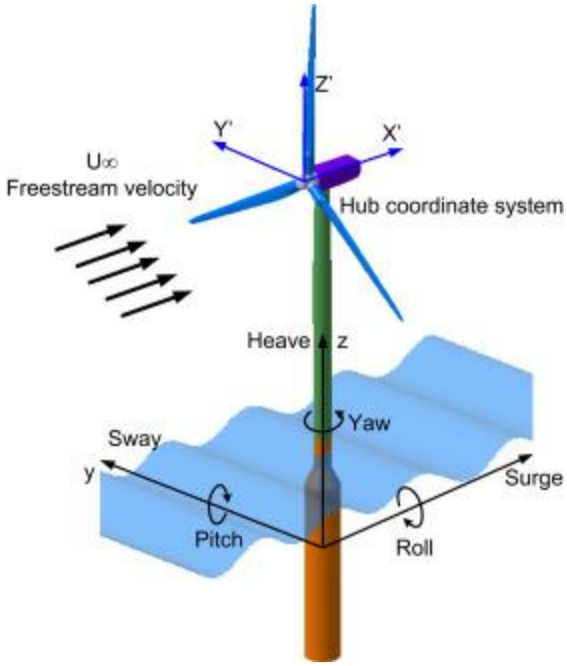

Figure 2: Six degrees of freedom (Tran & Kim, 2015)

The movement of entire floating structure is combination of these specific motions or degrees of freedom (DoF) and their amplitude would depend on the specific geometry of the floating structure (static loads) as well as on the interaction of the hydrodynamic and aerodynamic loads that are site dependent.

Lin, Wang & Vassalos (2018) explain that the 6 DoF contribute to creation of unsteady aerodynamics around the rotor, such as turbulent flow, rotor-wake interaction and rotor aerodynamic performance. In particular, yaw and pitch (rotational components) and surge (translational component) can to a large extent influence the platform motion. In their research, a Computational Fluid Dynamics (CFD) method was applied to analyze impact of the platform pitch and surge motions on the aerodynamic unsteadiness around the rotor. It was detected that the platform motion caused by these DoF creates “effective velocity” on the blades. The authors compared two modeling approaches: CFD and the Blade Element Momentum (BEM) that was used with the General Dynamic Wake (GDW) model, both applied on onshore and on the floating offshore wind turbines. The results showed the CFD was better suited to simulate complex flow field around the

FOWT than traditional BEM approach and that floating turbines require more advanced modeling tools than other types of wind turbines. CFD method demonstrated that there can be different results for power and thrust when the turbine was undergoing combined pitch-surge motions than when it was only in pitch or surge motion. The paper indicated that the future challenge for modeling tools would be to analyze multiple DoF at the same time in order to simulate FOWT responses accurately.

2.5.3 Vortex ring state

In analyzing impact of the platform motion, Sebastian & Lockner (2012a, 2012b, 2012c) and Sebastian (2012) as cited in Tran & Kim (2015) argued that the two most prominent DoF are yaw and pitch. The yaw and pitch motion create an unsteady aerodynamic field around the rotor leading to specific phenomena called “vortex-ring state”. The platform pitching motion activates rotor movement, which starts to pitch backwards creating some sort of self-induced turbulence, as illustrated in Figure 3.

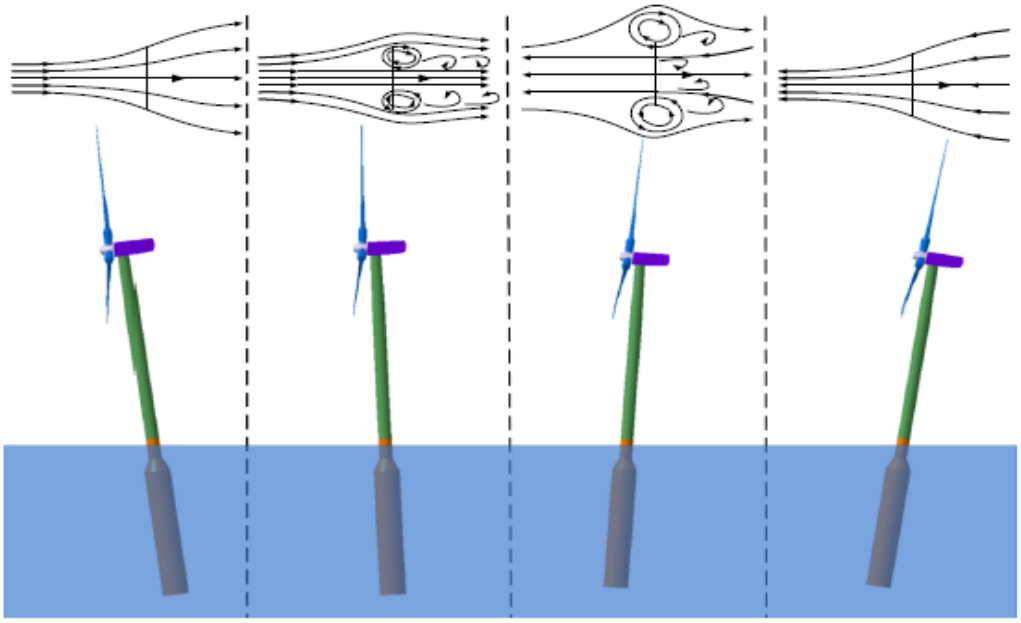

Figure 3: Impact of platform motion on the flow field (Tran & Kim, 2015)

Jeon, Lee & Lee (2004) used vortex lattice method to assess aerodynamic loads of the FOWT under specific pitch motion condition. Results showed that turbulent wake state

was created when platform was experiencing upward pitch motion. Due to upward pitching motion, the relative velocity of the tip of the blade became large leading to high tip speed ratio.

Liu et al. (2015) confirmed previous work in regards to modeling platform motion effects on the aerodynamic properties of the FOWT. The authors argued that if three DoF (surge, heave and pitch) were modeled simultaneously (which happens in real situations) there would be a better insight into the platform impact on the FOWT behavior. By using an open-source OpenFOAM numerical code, the authors demonstrated that the torque and thrust are strongly correlated to the platform motion. Similar to findings of Jeon, Lee & Lee (2004), it has been shown that when the turbine moves in downwind direction it interacts with its own wake which reduces vortices, and that moving into upwind direction intensifies vortices leading to creation of a turbulent wake state or a turbulent field.

In order to investigate aerodynamic load responses due to vortex-blade-interaction, Tran & Kim (2015) applied different numeric modeling techniques to compare the results. This involved an in-house developed unsteady blade element momentum (UBEM) Matlab code with a modified FAST AeroDyn code, an advanced unsteady computational fluid dynamics tool and the GDW method, applied on the NREL 5 MW reference wind turbine (developed by National Renewable Energy Laboratory - NREL). Direct local relative velocity method (DLRVM) and Equivalent Averaged Velocity Method (EqAM) were used in combination with the in-house UBEM tool to capture additional velocity experienced by each blade element due to the platform motion. All three types of codes were used to assess impact of the platform pitching motion on the aerodynamic power and thrust. The outcome demonstrated the good agreement of the results from all three codes in case of low pitching motion amplitude of 1-2˚. However, under bigger pitching amplitude of 4˚, which typically occurs in the normal wind and sea conditions, the differences in the resulting aerodynamic power and thrust were larger. Unsteady CFD method performed better as compared to other two numeric approaches and was capable of simulating transient turbulent field around the rotor including visualization of small

blade-tip-vortices. The method used in their research proved the correlation of vortex–blade-wake interaction, where the wakes were stronger during forward pitching motion (upstream) as compared to when turbine was moving backward (downstream), which was due to the bigger platform pitching amplitude.

2.6 Rotor-floater interaction

As shown in the previous section, the platform motion leads to rotor acceleration creating unsteady aerodynamics with variable power and thrust. Limiting pitch, roll and heave motion is directly related to reducing nacelle acceleration (Carbon Trust, 2015). Due to their geometrical configuration, the three main floating concepts have different abilities in restricting platform's DoF. Spar concept is in particular sensitive to pitch and roll motions, semi-submersible has rather high heave motion and TLP is the least susceptible to DoF motion due to its tensioned moorings and higher rigidity, which limits the vertical and lateral movement. Besides geometry, it is highly relevant to select an appropriate control mechanism and RNA for a floater. The rotor control mechanism can be effectively used to limit resonances and dynamic responses due to platform motion and in particular in case of large and irregular waves (Butterfield et al., 2007).

In conventional onshore wind turbine, the advanced control mechanism is basically used to optimize power yield, but also to reduce impact of the cyclical loadings imposed by the aerodynamic effects (wind shear, turbulence, wind gusts, etc.). With each revolution, the rotor blades are being exposed to periodic loadings that are not always the same per each cycle, which leads to rotor fatigue. Blade pitch control and smart rotor control are the most common methods used in advanced control mechanism to limit such loadings. In individual blade pitch control mechanism, each blade has its own pitch actuator and pitch angle that can be individually controlled. Collective blade pitch mechanism is applied by central controller for speed adjustment. Smart controller includes a number of control devices (such as trailing edge flap) that are placed along the blades for load reduction (Plumley et al., 2014).

Selection of an appropriate controller is even more complex for FOWT. The ability of each type of controller to limit platform motion and also aerodynamic loadings in FOWT has been intensively researched. Goupee, Kimbell & Dagher (2016) studied impact of the blade pitch and generator control on the FOWT by comparing different types of controllers with baseline case that had fixed blade pitch and rotor speed. The experiment demonstrated that active turbine controllers have overall positive effect in limiting loadings and motions of the floating structure. However, it should be noted that these beneficial effects may be offset by the increase in blade pitch actuation, variation of generator torque/thrust or alteration of rotor speed which altogether may increase loads on other turbine components.

Wakui, Yoshimura & Yokoyama (2017) argued that the platform motion and more specifically, pitch motion can cause additional fatigue loads on the FOWT, leading to unsteady power generation. The authors proposed a multiple feedback control method to reduce platform pitch motion and power fluctuation by using FAST. Multiple feedback method refers to a combined use of controllers: gain-scheduled generator power control with collective blade pitch manipulation and nacelle fore-aft speed control with the generator torque manipulation. It was argued that the combined use of controllers limits platform pitch motion and the variability of power output.

In a recent study, Ma et al. (2018) investigated the correlation of the wave prediction in designing an optimal control mechanism to offset the wave loading effects in the FOWT. It was argued that the feed-forward or Model Predictive Control (MPC) approach can be effectively used to mitigate the fatigue loads. The approach includes design of an overlaid optimal controller Linear Quadratic Regulator (LQR), which could reduce additional fore-aft tower base bending moment, based on predictive models for wave elevation and wave excitation forces. Although this method demonstrated good results, it should be noted that it created increase in the rotor speed variation and side-side bending moment, which has been an issue previously. It seems that this issue could not have been entirely eliminated when using rotor control mechanism to minimize platform induced motions.

2.7 Computer based tools for modeling FOWT

The accurate modeling of FOWT represents the most critical aspect for the floating offshore wind technology and the academia is closely collaborating with the industry in attempt to accurately predict the fluid-structure dynamics.

Modeling of FOWT has been mostly done by numerical simulation tools, because experiments in controlled environment inside water tanks proved to be rather expensive. Another problem with the tank modeling tests is that they usually rely on Froude scaling where Reynolds similarity law most often was not possible to confirm[6] and therefore they could not be extended to full-scale projects (Liu et al., 2017). The most commonly used computer aided engineering tools for numeric modeling of the FOWT's fluid-structure interaction (FSI)[7] in a time domain are aero-hydro-servo elastic codes.

2.7.1 Aero-hydro-servo-elastic codes

This type of simulation can well represent the structural response of solid parts of FOWT, such as platform, tower and blades when these parts are submerged in the surrounding fluid (gases and liquid). In this way, it is possible to capture non-linear dynamic behavior of FOWT covering aerodynamic loads, hydrodynamic loads, static loads, control system (servo) as well as electrical machinery effects. Aero-servo-hydro-elastic codes consist of several models/solvers which deal with each FSI component separately.

Finite Element Momentum (FEM) theory is applied in simulation of complex structural responses of the floating structure. FEM is used in the finite element analysis to solve numeric model equations as an approximation of solving partial differential equations (PDE), in order to explain certain physical phenomena, such as fluid structure

[6] Reynolds similarity law states that in any model two geometrically similar flows are equal as long as they can agree on the same Reynolds number, which is a dimensionless quantity in fluid dynamics.

[7] FSI refers to interaction of a movable structure (floating turbine) with the surrounding fluid such as water and air.

interaction, electromagnetic problems, thermo-chemo-mechanical problems, biomedical engineering issues, etc. (Simscale, 2018).

For simulation of flow around the rotor, aero-elastic codes are usually coupled with either BEM or CFD method. *Blade Element Momentum (BEM)* theory is combination of *the blade element theory,* which is based on calculation of the forces that act along the blades and *the momentum theory,* which is based on calculation of induced velocities around the rotor flow field (Moriarty & Hansen, 2015). BEM has been used with various aero-servo-hydro elastic codes to simulate aerodynamic performance, energy optimization and the control system in conjunction with the empirical engineering model corrections to account for unsteady effects of the flow field. CFD tools will be considered in more detail in the next sub-section.

Most of the currently available aero-servo-hydro-elastic codes have evolved following the baseline model of NREL's FAST code (Fatigue, Aerodynamics, Structures & Turbulence) and integrating a specific hydrodynamic module for analysis of coupled effects of the floating turbine. Such examples include FASTv8/ OpenFAST, developed by NREL; Bladed, developed by DNV GL; HAWC2, developed by DTU; 3DFloat, developed by Nygaard (Shen et al., 2018).

In academia, FAST has been widely used mainly because it is an open source, non-commercial software, which showed good results in modeling FOWT dynamics. Its Hydrodyn module has been effectively integrated within FAST platform to compute hydrodynamic loadings, but there are doubts if the damping model can accurately simulate responses in transversal direction due to vortex shedding (Liu et al., 2017). For modeling aerodynamic performance, FAST AeroDyn Model uses BEM theory, but several comparative experiments with BEM showed that it was not fully capable of predicting dynamics of unsteady flow field and failed to accurately forecast aerodynamic loads (Sebastian & Lackner, n.a. as cited in Shen et al., 2017). Some researchers used "vortex methods" for improved 3D analysis of flow development around the rotor and wake interaction, but this type of modeling tends to disregard viscous effects that are important for understanding dynamics of flow separation (Liu et al., 2017).

2.7.2 Computation Fluid Dynamic (CFD) tools

CFD tools are based on solving Navier-Stoke equations to simulate the interaction of fluid flows within defined boundary conditions (grid mesh). CFD methods can calculate fluid viscosity and hydrodynamic drag forces in FOWT which gives more accurate results in modeling flow field. Downside of this type of tools is that computation is often time consuming and rather complex so that most of the researchers apply restrictions and do not take into account the full aerodynamic properties or platform's DoF motions (Liu et al., 2017).

Among different CFD tools, OpenFoam is so far widely used because it is free and an open source toolbox, which consists of several numerical solvers for analyzing and predicting complex fluid dynamics of the floating structure.

2.8 Research gap

Floating offshore wind turbine represents a complex system which requires exceptional modeling and testing resources. As shown in the literature, for an accurate analysis of FOWT, different aspects of its behavior need to be considered simultaneously such as floater-rotor interaction, impact of the mooring and anchoring system, loading effects and structural responses. Researches commonly rely on coupling two or more numerical simulation techniques because tank test and demo projects are quite expensive. It is also questionable to what extent coupling can fully capture floating system and its complex features. In most cases, there is a tendency to reduce simulating parameters (such as number of degrees of freedom) or to concentrate on one specific aspect (vortices, wakes, hydrostatic stiffness, or rotor control). The comparison of energy yield between the spar and the semi-submersible floating concepts has been addressed to a limited extent in the scientific literature. The researchers mainly concentrated on understanding one or another concept in order to further improve the specific design. Therefore, the present work represents an ambitious attempt to tackle this issue using a less computationally demanding modeling tool which can capture most of the FOWT features.

Chapter 3

Methodology

This section will describe a methodology which will be applied to answer the research question and to test the hypothesis. The method is based on the numeric modeling that would follow the ASHES configuration. After introducing the methodology framework, the baseline properties and validation of the code will be presented and the six load cases defined. This is followed by a description of how the environmental loads, floaters and rotor are modeled. Finally, a method for calculation of AEP and power output will be described in the last section of this chapter.

3.1 Methodology framework

As explained in Chapter 2, the floating wind turbines are subject to larger and more composite loads as compared to conventional onshore and bottom fixed offshore turbines. The loadings acting on a moving platform that carries the rotor can trigger the system responses which then affect the field around the rotor and eventually, the turbine energy output.

Approach to the method used in this work starts from the perspective of a floating wind farm developer in the initial, planning phase of a project, who wants to get a better insight on what is the impact on energy yield from loads-floater interaction and which type of floater may therefore have advantageous performance. For any future floating wind farm project, the accurate power curve that fully takes into account effects from

loadings would be indispensable part of initial analysis before the project could actually move on. As shown in the previous chapter, such an analysis would normally involve use of two or more advanced numerical modeling tools that can be resource demanding to a project developer who often needs a fast feedback in the initial project phase.

A simplified method as illustrated in Figure 4 is therefore proposed to address this issue:

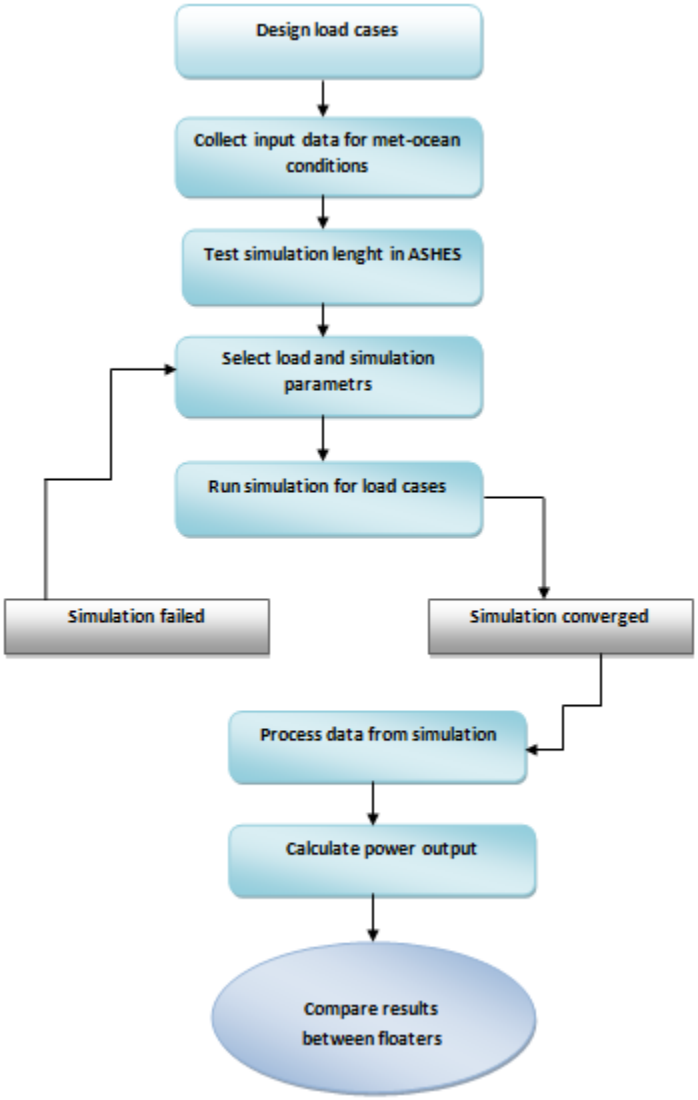

Figure 4: Methodology flowchart

The analysis performed under this paper will be based on numerical methodology defined in ASHES. For both type of floaters, the properties of baseline offshore NREL 5 MW (Jonkman et al., 2009) turbine will be used in simulation of 6 load cases. Only environmental parameters will vary per each load case, while the general parameters related to platform system, rotor, simulation type and length will be set up initially and kept constant with slight adjustments. The modeling of environmental conditions will be performed by using online data available for the case study site: UTSIRA NORD (Category A). After simulation is finished, the power output will be analyzed per each load case and results discussed.

3.2 Modeling tool: ASHES

ASHES stands for aero-servo-hydro-elastic simulation software with 3-dimensional spatial visualization. It was developed by SIMIS AS, a spin-off company created in 2013 from the Norwegian University of Science and Technology (NTNU). The software was launched with an aim to assist a wide range of users in a study and design of onshore, offshore-fixed and offshore floating wind turbines by advanced visualization graphics and computational efficiency under the motto "*Wind turbine design with superpowers*". The version used in current work is 3.3.1, which was released in July 2018 with improved platform for simulation of the floating offshore wind turbines.

ASHES is configured as a FEM platform which is used for structural (elastic) modeling. FEM comes together with the co-rotational formulation of beam elements (Euler-Bernoulli with 12 DoF) that are interconnected with the computational nodes. In particular, the floating structures are modeled as flexible bodies, which is necessary for obtaining accurate eigenfrequencies of entire system to reflect its dynamic responses (transfer of loads, stress, damping, etc.).

The software is based on model templates that can be tailored per a specific load case which needs to be analyzed. This means that pre-defined solvers for solution of linear and non-linear equations are embedded in the system which selects a suitable option

depending on the input model and loads specifications. For example, for solving equations of motion, the Newton-Raphson[8] model (also known as Newton's method) will address non-linear effects while linear equations are applied in cases of linear (predictable) motion (ASHES, 2018). Equations of motions are used in numerical analysis to describe movement of the structure as a function of time. Dynamic motion of the turbine is solved by calculating forces and energy of the particles at different positions taking into account spatial coordinates. This is performed using the Newton's method through a system of non-linear equations.

Aerodynamic loads are modeled based on the BEM theory, with Glauert's correction and Prandtl's tip-hub-loss correction, coupled with the structural responses. Wave kinematics are solved by using $Airy_{str}$ (Airy theory with stretching method) while hydro loads (based on wave kinematics) are calculated using Morison's equation (ASHES, 2018). The control (servo) loads are solved by DLL (Dynamic Link Library) with internal control system (Popko et al., 2018).

Due to such configuration, it is possible to perform the integrated analysis of a full floating wind turbine system:

- Time domain analysis
- Solutions of eignefrequencies of system responses
- Structural, aerodynamic and hydrodynamic loadings
- Rotor control mechanism
- Blade and airfoil properties
- Platform, tower, mooring and anchoring characteristics
- Electrical machinery properties
- Displacements

The user interface is visually advanced and straightforward with pop-up menus that explain in a nutshell what are the parameters and which are the default and min/max values (where relevant). Live sensors with values and graphical visualizations in time

[8] Mathematical model of finding better approximation to the roots (or zeros) of a real valued function.

simulations are supporting tool for monitoring changes per specific parameter which needs to be analyzed. An example is given in the Figure 5, which depicts the load case IEC EWM (extreme wind speed) in the time simulation mode. Values of the generator sensor (right side) are read for specific time in the simulation clock while live graphs show sensor values per time change (left bottom corner). Resulting values can be exported in form of .txt file and visualized as graphs.

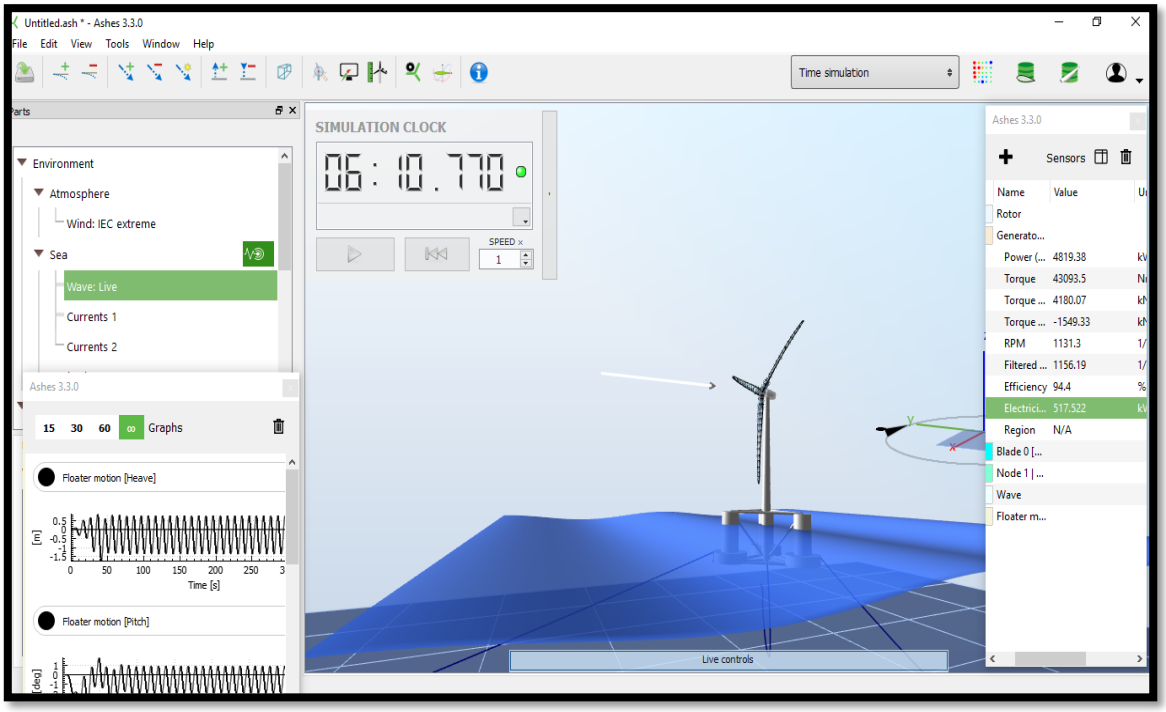

Figure 5: Example of ASHES user interface (ASHES, 2018)

The simulation can be performed in 4 different ways:

- ***Time simulations*** where duration of simulation can be set up and controlled by the user and different load parameters can be changed in live mode;
- ***Rotor characteristics simulation*** creates thrust and power coefficients based on the mean reference wind speed, Tip-Speed-Ratio (TSR) and range of wind speed for reference rotor, but without considering impact of floater motion and tower;

- ***Eigenmodes simulation*** is used to examine a specific range of the eigenfrequencies and to visualize the displacements of different parts of the floating structure;
- ***Batch analysis*** is used to simulate in parallel a set of load cases with different parameters to check some specific value and to reduce overall simulation time.

3.2.1 Validation of the code

The validation and benchmarking of ASHES has been running in parallel with its development, which started in 2012. After each validation exercise, the code has been further improved. The BEM of the code was tested through NORCOWE/NOWITECH Wind Tunnel Blind Test, which showed overall a good agreement with other BEM and CFD models (Thomassen et al., 2012). The power curve under this benchmarking test is shown in Figure 6, where ASHES is represented by Suja & Thomassen (BEM).

In the process of further development, ASHES became part of Offshore Code Comparison Collaboration Continuation (OC4) with Correlation (OC5) projects. Both are continuation of OC3, a large project launched in 2005 by International Energy Agency (IEA) Wind Task 30, with an objective to verify and validate performance of aero-hydro-servo-elastic modeling tools for offshore wind turbines. In OC4 project, ASHES results have partially validated unsteady BEM method (Thomassen et al., 2012).

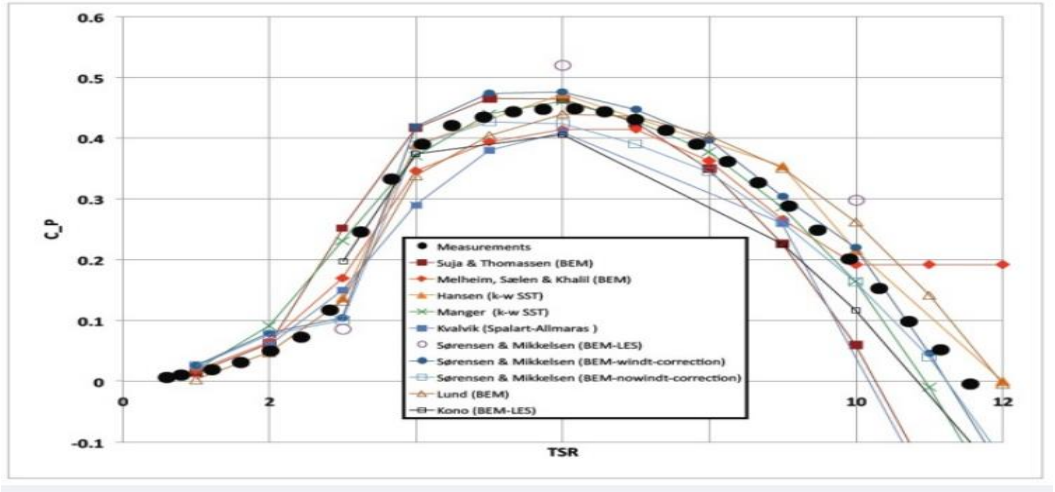

Figure 6: Power curve, ASHES / Suja&Thomassen (Krogstad & Eriksen, 2011)

In the next step, OC5 phase was carried out to verify results from the simulating codes with the actual tank test responses (Phase I and II). The Phase III was launched to validate responses with the reference turbine (Senvion 5 MW) installed at the Alpha Ventus Offshore Wind Farm in the North Sea. It involved several participants from the industrial and academic fields from 12 countries (Popko et al., 2018).

Due to the limitations related to intellectual property rights, in the Phase III the participants had to use NREL 5 MW instead of real blade design and full controller data from Senvion 5 MW. The Phase III concentrated on the responses from the support structure to analyze displacements and forces. The experiment included 4 different load case scenarios: the first one analyzed mass and structural forces; the second group dealt with the stiffness by examining interaction between rotor-nacelle-assembly and the floating structure; third and fourth load scenarios investigated turbine and controller performance under stepwise and turbulent wind cases. The simulation of the load cases was run several times, during which the participants had opportunity to adjust their models to the real responses from the Senvion turbine (Popko et al., 2018).

4Subsea was a Norwegian company that participated in the project using ASHES. The selected load case data showed overall good match between the results of participating modeling tools (including ASHES) and the real turbine responses for most of the load cases. The largest discrepancy was found for the load cases 3 and 4, simulated under the stepwise wind to analyze transient response in all operating wind speeds with 1 m/s step difference and 50 s time length. The results from stepwise modeling (Figure 7) were overall in agreement with the reference turbine for the partial-loading (6-8 m/s) and for full-load operating regime (16-18 m/s), but not in the range between 8-13 m/s (Popko et al., 2018).

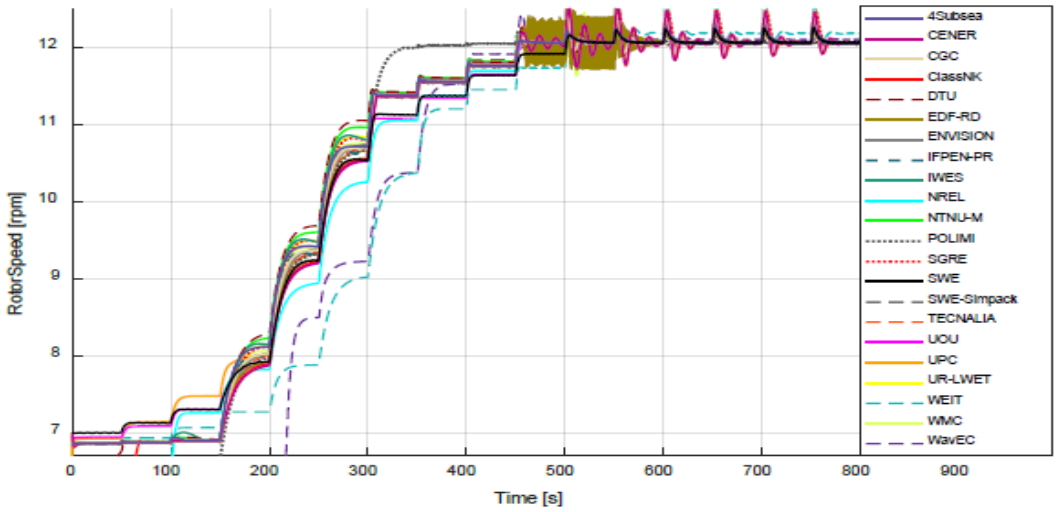

Figure 7: Rotor speed under stepwise wind, ASHES/4Subsea (Popko et al., 2018)

In the operating range 8-13 m/s, rotational speed of the rotor tends to be larger than the one in real life for majority of codes. However, in the OC5 Phase, ASHES was benchmarked and validated for offshore wind turbine in most of the selected load cases except for the verification of rpm in the operating range between 8-13 m/s. This is explained by the difference in blade design used by modeling tools and the blade properties of actual, physical turbine of Senvion (Popko et al., 2018).

3.3 Numerical simulation

3.3.1 Modeling atmospheric conditions

As indicated earlier, ASHES aerodynamic modeling is based on BEM theory with Glauert's and Prandtl's correction. However, airflow properties such as frequency distribution of wind speed and direction, turbulence, wind shear, wakes, air pressure, temperature, etc. cannot be simulated at the same time in this code. Instead, separate wind file should be created per each load case with different combination of wind and air parameters which ASHES solves automatically using one of its system algorithms.

There are six options available for modeling wind field in ASHES: live, uniform, IEC extreme, sine, stepwise and turbulent. In the current analysis only stepwise, turbulent

and IEC extreme wind will be used, while the rest were not considered as relevant to this research. Stepwise wind is the fastest way to create the power curve, which is the main reason why it was chosen as a baseline wind option but also to test floaters at normal wind operating conditions. Turbulent and IEC wind models were selected to analyze stochastic and extreme aerodynamic effects on the floating turbine.

There are 6 load cases that will be simulated for each floater separately in the *Time Simulation* mode. This mode was selected as the most appropriate one, because of the possibility to control timing and ability to use full-scale parameters to model the entire floating structure. The set-up of load cases is explained in the following sections, whereas detailed data for environmental modeling is presented in Chapter 4 (*Application of the Methodology*). Input parameters for all load cases are given in Appendix 1.

3.3.1.1 Stepwise wind

The stepwise wind file is created with the wind speeds ranging from 0-25 m/s and used for LC1, LC2, LC3 (Appendix 2). This option allows an accurate simulation of time which elapses between each change of the wind speed. LC1, LC2 and LC3 represent respectively the mild, mean and rough load cases as combination of stationary values of site related climate conditions. The input for simulation is a wind file which contains wind speed and wind directions data divided in several time steps, each with a specific value. The wind flow under this option is assumed to be steady and uniform in the given time step duration range (before each time step change). Under stepwise wind, it was observed that the sudden changes of wind speed over a short time (several seconds) can cause transient effects that can distort the power output. After several trials, it was decided to increase duration of the time step between each change of the wind speed to more than one minute as compared to default value of 10 s as to get stable results.

The bigger time step was allowed (500 s) at the start of the simulation and before the turbine begins producing electricity, to limit transient effects on the rotor after which the time step is reduced to 150 s for 4-25 m/s range. The wind direction is kept constantly at 0˚ because the wind turbine faces the north by default in ASHES, which is sufficient for

this type of analysis, since there was no option to enter frequency distribution of wind speed and wind direction.

For each load case, the stepwise wind conditions (speed, direction, duration of time steps) were assumed to be constant at the rotor hub. Effects of turbulence including vertical wind shear and roughness length are not considered in the analysis of stepwise wind as the software does not give that option.

3.3.1.2 Turbulent wind

For the purpose of analyzing the stochastic effects of turbulence and wind shear on the floaters, the turbulent wind load cases LC4 and LC5 were designed. In an offshore environment, the turbulence and wind shear can be important under more severe environmental conditions. ASHES uses NREL TurbSim Stochastic Inflow Turbulence Simulator for modeling a turbulent wind (Kelley & Jonkman, 2007). NREL TurbSim Simulator is designed for numerical simulation of coherent turbulent flow field that is characterized by spatiotemporal turbulent velocity field, which is typical property of the flow in an unstable boundary layer. It is based on the NREL National Wind Technology Center Upwind (NWTCUP) spectral model that generates turbulent inflow according to NREL's test results of turbulent load cases.

The TurbSim effectively creates "randomized" coherent structures, which are "superimposed" on one of the arbitrarily created turbulent fields, generated by specific spectral model, such as SMOOTH (used for homogenous, flat terrain) WF_UPW, WF_07D, WF_14D (used for upwind flows of multi-row wind farm and 7-14 rotor diameters spacing) and IEC Kaimal and von Karman normal turbulence model. However, it should be noted that such "superimposed coherent structures" can trigger transient loading effects on rotors and structures.

The average wind speed at the hub height in our simulation (90 m) is automatically computed in ASHES using power law formula:

$$V(z) = V(z_r) * \left(\frac{z}{z_r}\right)^{\alpha} \quad (1)$$

where z is height above ground, z_r is the reference height above ground and α is wind shear exponent.

In the current analysis, LC4 is set up as Normal Turbulence Model (NTM) based on IEC Kaimal NTM, while LC5 is configured as Extreme Turbulence Model (ETM) in line with the IEC extreme Kaimal ETM, which are two model options available in ASHES.

For floating wind turbines, the grid size needs to be rather large because high loads tend to move the rotor outside the wind field. Therefore, a grid size of 40% to rotor margin will be used for LC4 (NTM) model with the grid points 40x40. In case of LC5 (ETM) the grid size will be bit larger with 40.26% rotor margin and grid points 45x45, because larger loads need to be simulated.

Figure 8 visualizes wind turbine operating under turbulent wind field. Changes in turbulence regions that form turbulent wind field can be observed and tracked in regards to time change.

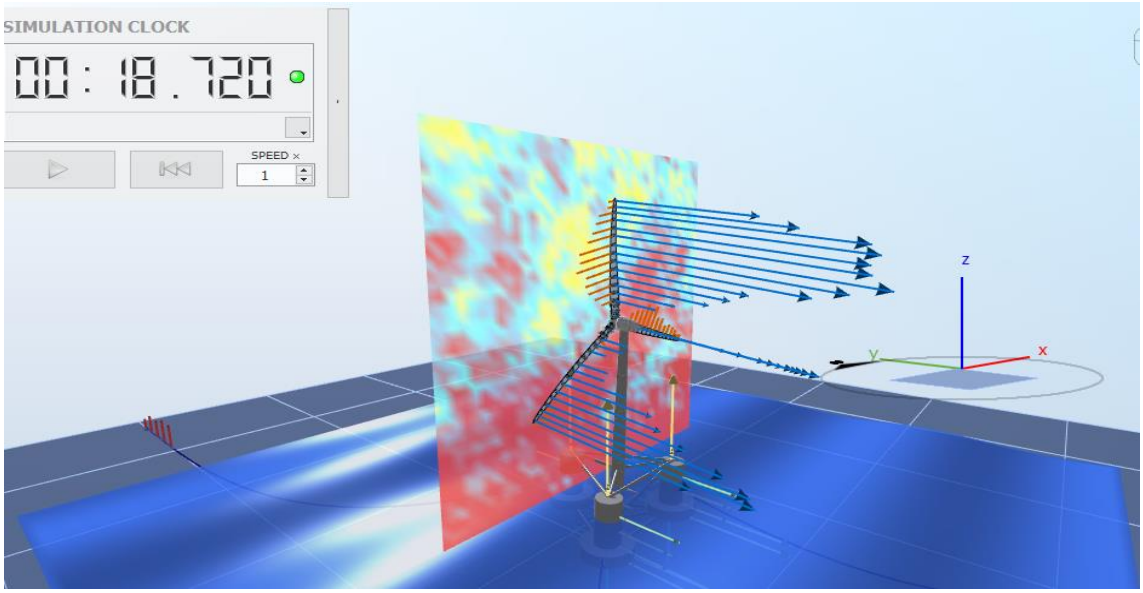

Figure 8: Semi-submersible floating turbine under turbulent wind (ASHES, 2018)

3.3.1.3 Extreme wind

One of the IEC 61400-1 load cases can be selected in ASHES to test the performance of a wind turbine in extreme conditions. Available models are: ECD (extreme coherent gust with direction change), EDC (extreme direction change), EOG (extreme operating gust), EWM (extreme wind speed), EWSH (extreme wind shear horizontally), EWSV (extreme wind shear vertically).

Under current analysis, the extreme load case will be tested using Extreme Wind Speed (EWM), which according to IEC 61400-1 standard can be modeled as either steady or turbulent extreme wind (steady extreme model was selected for our simulation).

Extreme wind speed with the recurrence period of either 50-year or 1-year is defined as function of z:

$$V_{e50}(z) = 1.4\, V_{ref}\,(z/z_{hub})^{0.11} \qquad \textit{(50-year recurrence)} \qquad (2)$$

$$V_{e1}(z) = 0.8\, V_{e50}(z) \qquad \textit{(1- year recurrence)} \qquad (3)$$

EWM is modeled without wind shear, where mean wind speed is assumed to be constant at the rotor hub. It was also assumed that ASHES simulates extreme wind speed with 50-year recurrence period.

3.3.2 Modeling ocean conditions

Ocean loads are modeled in ASHES using Airy theory and kinematic stretching. Airy wave theory is linear theory which explains fluid motion of regular, periodic and 2-dimensional waves where particles are modeled by “superposition” (Burton et al., 2011).

When Airy theory is applied, there are no modifications to water particles that occur due to elevation of mean water surface. However, when non-linear fluid motion needs to be modeled, other theories are used to capture irregular and bigger waves and modifications of particles (such as kinematic stretching).

ASHES uses Wheeler algorithm for computing non-linear kinematic stretching of waves (stretching is illustrated in Figure 9). According to Wheeler stretching method, the velocity of fluid at still water level is considered to be reduced as compared to linear

theory (Det Norske Veritas, 2010). At certain free surface elevation level, the fluid velocity is calculated using linear theory for each frequency component and for each time step in time series a vertical coordinate (z) is stretched as follows:

$$z = \frac{z_s - \eta}{1 + \frac{\eta}{d}} \quad ; \quad -d < z < 0;\ -d < z_s < \eta \tag{4}$$

where z_s is the stretched z-coordinate, η is the free surface elevation and d is the mean water depth.

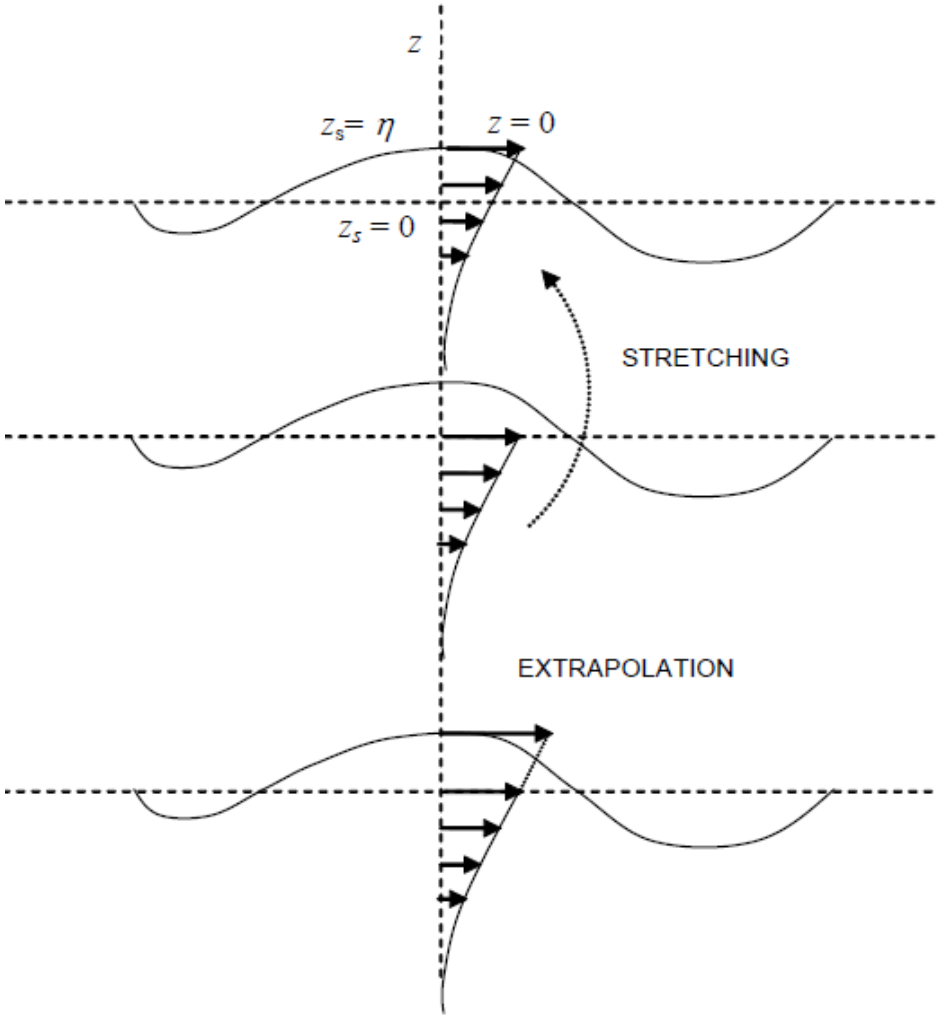

Figure 9: Stretching of wave velocity profile (Det Norske Veritas, 2010)

Wave kinematics modeling can be supported by ramp-down option in ASHES to improve numeric stability and better reflect kinetic behavior of particles at a certain distance under the sea level where it occurs. There is also an option to include deep water kinematics to improve kinematic modeling.

In ASHES, waves can be modeled as live (user defined), regular, irregular with single spectra and irregular with double spectra (combination of sea wind and swell). The currents can be modeled as either linear (Airy wave theory) or kinematic stretching (based on Wheeler algorithm).

3.3.3 Modeling hydrodynamic loads

There are two main theoretical approaches to describe hydrodynamic loads imposed on floaters: potential flow theory and the Morison's equation, depending whether the flow separation occurs along the upper part of the platform or not. If there is no flow separation, the potential flow theory applies. Potential flow theory is generally used in fluid dynamics to describe motion of the continuum as velocity field that is mathematically represented as vector field and a gradient of scalar function.

However, for cylindrical structures, hydrodynamic coefficients depend on the Keulegan-Carpenter number (K) and Reynolds number (Re) which increase with sea severity and decrease with sea depth (Robertson et al, 2014). Dimensionless numbers *K* and *Re* are defined as

$$K = \frac{uT}{D} \tag{5}$$

and

$$Re = \frac{uD}{v} \tag{6}$$

where *D* is cylinder diameter, *v* is kinematic viscosity of fluid, *T* is wave period and *u* is amplitude of fluid velocity normal to the cylinder.

In conditions when K is bigger than 2, a flow separation occurs, which happens for the spar only in case of severe sea state (due to its smaller upper part of platform) and in case of the semi-submersible, the flow separation happens in most of the sea states (moderate to severe). When the flow separation occurs, additional loads in surge, sway, roll and pitch directions need to be represented in the potential flow theory (if this theory is to be used) by additional linear damping.

However, in the sea conditions when the flow separation occurs, which is usually in moderate to severe sea states, a "simplified" Morison's equation is commonly used to describe the flow structure interaction. As indicated by Robertson et al. (2014), most of the wind turbine codes use Morison's equation to model hydrodynamics for all sea states rather than potential flow theory, because of the complexity to fully model additional loads due to flow separation. The Morison's equation is also used by ASHES in modeling hydrodynamics of floating wind turbines.

The Morison's equation is considered as an appropriate method to describe hydro loads in both NREL baseline floaters[9], in the most sea states where hydrodynamic loads are created by wave forces such as wave excitation, radiation damping, flow separation and additional mass loads. Morison's equation can capture in a simple form diffraction effects from long wavelength theory from moderate to severe sea states; the radiation damping in the most cases is not important and the flow separation occurs in upper parts of both floaters (Robertson et al., 2014).

The Morison's equation describes total forces exposed on cylindrical structure (platform) per unit of length in a transverse flow:

$$F = \frac{1}{2} C_d \rho D (u - \dot{q}) |u - \dot{q}| + (1 + C_a) \rho \frac{\pi D^2}{4} \dot{u} - C_a \rho \frac{\pi D^2}{4} \ddot{q} \qquad (7)$$

[9] Both spar and semi-submersible floaters used in current analysis are based on NREL baseline models as defined in Section 3.4.

Where:

C_d = drag coefficient

C_a = added mass coefficient

D = diameter of cylinder

$\dot{q}$ = first time derivative of cylindrical structure velocity

$\ddot{q}$ = second time derivative of cylindrical structure velocity

ρ = fluid density

u = fluid particle velocity

$\dot{u}$ = first time derivative of fluid particle velocity

3.4 Floater properties

In ASHES, default values of both floaters follow by most part the baseline characteristics as originally developed by NREL, with slight modifications of semi-submersible floater. Mooring and anchoring system default values were kept constant as configured in ASHES and their structural details are given in Appendix 3.

3.4.1 Properties of the semi-submersible floater

Baseline concept for semi-submersible floating system was developed under the Phase II of the Offshore Code Comparison Collaboration Continuation OC4 project (Robertson et al., 2014). Configuration of NREL semi-submersible floater is based on the *DeepCwind* model. The platform consists of three offset columns and central (main) column interconnected with each other by number of pontoons (Figure 10). Entire platform is partly submerged. Each offset column has larger diameter cylinder (base column) which serves to limit the platform motion mainly in heave direction but also in surge, sway, pitch and roll directions. Offset columns are ballasted with the water in the lower parts (Robertson et al., 2014).

Figure 10: DeepCwind semi-submersible floater (Robertson et al., 2014)

At the bottom of the columns there are entrapment (heave) plates, which add to mass and hydrodynamic inertia of the system and limit the platform motion by increasing viscous damping in the pitch, heave and roll motion. Given its geometric and hydrostatic properties, it has great stability and can operate in shallow water depth (Bagbanci, Karmakar & Soares, 2015). Baseline properties of semi-submersible floater are provided in Appendix 3.

3.4.2 Properties of the spar-buoy floater

The spar-buoy concept emerged under the Phase IV of the Offshore Code Collaboration project OC3 (Jonkman, 2010). The floater is modeled according to Statoil's *Hywind* design. It consist of a long pile draft, whose lower part is submerged in water and much longer (-120 m) and a smaller upper part which is 10 m above the water (Jonkman, 2010). The lower part (draft) is larger or same as the upper part above sea water level (when tower included), which is designed to limit the heave motion (Figure 11). Due to its large submerged draft it requires higher water depth, and this type of floater is best suited among all three concepts for the very deep waters (Bagbanci, Karmakar & Soares, 2015). Details of spar buoy floater are given in Appendix 3.

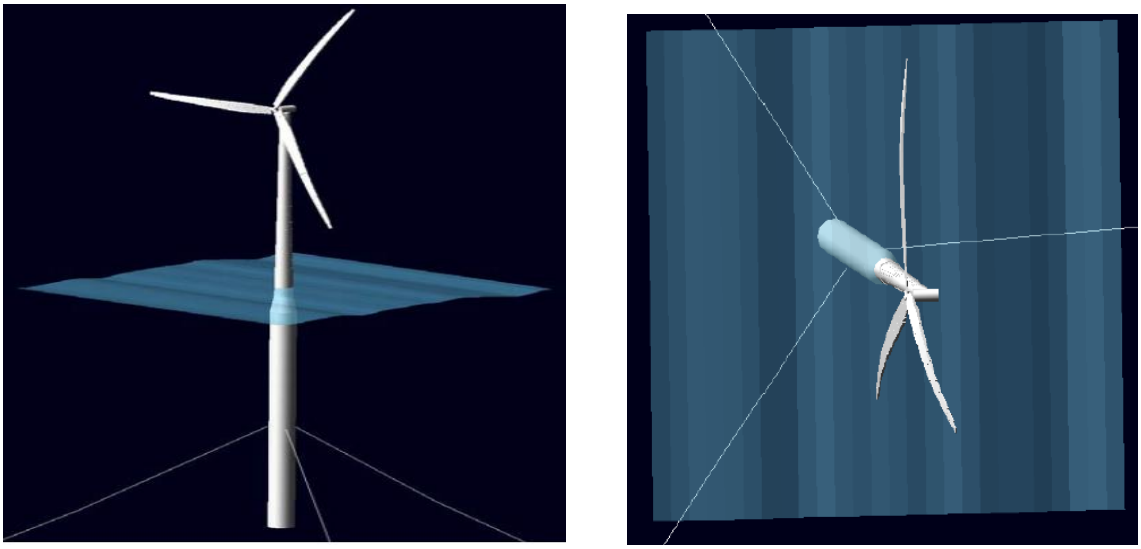

Figure 11: Hywind spar floater (Jonkman, 2010)

3.5 Rotor and controller characteristics

Due to its accessibility as open source data, the properties of the NREL baseline 5 MW offshore wind turbine will be used as input data in modeling rotor dynamics. The NREL 5 MW is 3-bladed horizontal axis wind turbine, with the variable speed and variable pitch-to-feather-control. However, the traditional variable speed controller cannot be used for floating wind turbine systems as it may trigger negative damping and provoke big resonances when the rotor thrust is being decreased after the turbine enters in the above-rated wind speed regime. As indicated by numerous research, for floating wind turbines it is very important that the platform-to-pitch damping (ratio) remains positive and large (Robertson et al., 2014).

To address this problem in both OC3 (spar) and OC4 (semi-submersible) concepts, the NREL designers made specific changes to the rotor controller:

1) Controller-response natural frequency was decreased to 0.2 rad/s below the platform - pitch natural frequency of 0.21 rad/s (also lower than wave excitation frequency in most of the sea conditions) to preserve a positive damping of the

support structure. In this way, the gains from blade-pitch-controller were reduced to ensure system stiffness and stability.

2) Control law in region 3 was modified to make generator torque constant at 43,093.55 N/m, instead of keeping the power constant. This change would limit rotor-speed exaggerations and negative damping, but there can be some overload in generator when power gets bigger at above rated wind speed.

These modifications are incorporated in the control system Dynamic Link Library (Robertson et al., 2014) and used in ASHES as external OC3 Phase IV controller.

Overview of fundamental properties of the NREL 5 MW turbine as used in ASHES is given in Appendix 3.

3.6 Method for power output calculation

Reliable estimate of annual energy production (AEP) is a decisive element for viability of any wind farm project. The assessment of annual energy electricity production is based on the power curve performance. In its basic definition, the power curve represents electricity output, which depends on turbine technical specification and the wind speed regime at the site. The turbine technical properties are characterized by the aerodynamic efficiency of the rotor, the maximum installed generator capacity, the rotor control system and the mechanical and electrical efficiency. Aerodynamic efficiency of the rotor is measured as power coefficient of rotor (C_{PR}), which is around 50% in the modern 3-blade horizontal axis turbine, close to Betz's theoretical maximum of 59.3%[10]. Besides rotor power coefficient, the assessment of the wind turbine electricity production should include mechanical and electrical losses incurred due to energy conversion system, i.e. drive train efficiency ($\eta_{\text{mech.-electr}}$). Hau (2013) defines combined

[10] Based on the Betz's Elementary Momentum Theory, the optimal power that can be extracted from the free airstream velocity is given by the ratio of the flow velocity before it intersects a given cross-sectional area (turbine rotor) and the flow velocity after the cross-sectional area. The optimal ratio is C_{PR}=16/27 or 59.3% and is referred to as "ideal power coefficient" or "Betz coefficient".

rotor and mechanical-electrical efficiency as turbine's power efficiency (CP)[11], which is used in calculation of the electrical power output (P_{el}):

$$P_{el} = CP \frac{1}{2} \rho A v^3 \quad (8)$$

where CP is the power coefficient of the turbine ($CP = C_{PR} * \eta_{mech.-electr.}$), ρ is air density in kg/m^3 (default value is 1.225 kg/m^3), v is the wind speed (m/s) and A is rotor swept area per m^2. P_{el} is expressed in W ($1\ W = \frac{kgm^2}{s^3}$).

The power curve is represented as a graph that shows how large is the electrical power output at different wind speeds. It consists of the following basic elements:

- Cut-in wind speed at which the turbine starts producing electricity (at 3 or 4 m/s)
- Rated operating wind speed (between 12-15 m/s)
- Cut-out wind speed (around 25 m/s)

The wind turbine generates its maximum power at the rated operating wind speed, when it reaches its installed capacity, i.e. the maximum generation of electrical power that can be sustained in a continuum over time. As noted by Hau (2013), the rated power cannot be exactly obtained in practice, but is rather "rounded" value, because it depends on the site-specific conditions (such as turbulence) and the type of the rotor controller.

For AEP calculation, it is necessary to know a power curve and a wind regime at the hub height per given site. Wind regime is obtained either via site measurement campaigns or via statistical methods such as annual wind speed frequency distribution. In the present analysis, we will use statistical techniques to determine wind speed regime. A commonly used method to assess how the wind velocity is distributed is a Weibull probability density function (Manwell, McGowan & Rogers, 2009):

---

[11] Note: Hau used "C_p" (lower index "p") to describe power coefficient of turbine, but we will use here the capital "P" for CP to differentiate it from the capacity factor "$C_{p''}$, explained later in this section.

$$\phi(v) = \frac{k}{c}\left(\frac{v}{c}\right)^{k-1} e^{-\left(\frac{v}{c}\right)^{k}} \quad (9)$$

where $\phi(v)$ is probability density function of the wind speed, *k* is Weibull shape factor, *e* is logarithmic base (normally natural logarithm, e = 2.781) and *c* is Weibull scale factor. The Weibull scale factor is derived by re-arranging mathematical expressions of probability density function and Gamma function[12] and depends on the mean wind speed (v_m):

$$c = \frac{2v_m}{\sqrt{\pi}} \text{ or } \approx 1.128\text{v} \quad (10)$$

The *k* - parameter represents shape of the frequency curve, which can take value of 1, 2 and 3. When only a mean wind speed is known, it is recommended to use the *k* - factor of 2 and the Weibull probability density function then becomes a Rayleigh probability density function:

$$\phi(v) = \frac{2\text{v}}{c^2}\, e^{-\left(\frac{v}{c}\right)^2} \quad (11)$$

If the shape of the frequency curve takes value of 2, the frequency distribution is assumed to be characterized by continuous wind speeds and some periods of lower or higher winds that is near to real distribution of wind statistics for most of the sites (temperate latitudes).

When the wind regime probability density function, $\phi(v)$, and the power curve, $P_{el}\,(v)$ are known an average wind turbine power output can be calculated by the following expression (Manwell, McGowan & Rogers, 2009):

$$\bar{E} = \int_0^{\infty} \phi(v) * P_{el}\,(v) * dv \quad (12)$$

[12] Gamma function is extension of factorial function defined for all complex numbers but non-positive integers as $\Gamma = \int_0^{\infty} x^{z-1}\ e^{-x}\ dx$ (also know as Euler integral of second kind).

where $dv =$ wind speed interval (width of bin), usually 0.5 m/s or 1 m/s. In the present analysis interval is assumed to be 1 m/s or $dv = v(i) - v(i-1)$.

In ASHES, the aerodynamic power from the rotor is obtained as a product of the aerodynamic torque (from BEM) and the rotational speed of the rotor. Similarly, the generator (electrical) power is automatically calculated by software as a product of generator torque and rotational speed of the main shaft, where torque is set by the controller.

In the current analysis, the AEP will be calculated for 3 stepwise load cases based on the values of electrical (generator) power obtained from ASHES at specific time step per each change of the wind speed (with the interval of 1m/s), starting with cut-in wind speed 4 m/s (v_{ci}) until cut-out wind speed 25 m/s (v_{co}).

Hence, the AEP is calculated as a sum of products of electrical power output and the fraction of Rayleigh distributed yearly hours of wind speed from cut-in to cut with the velocity distribution range of 1m/s ($\Delta\, v$):

$$AEP = \sum_{vci}^{vco} \ \phi(v) * P_{el}\,(v) \ * \ 8760\ h * \ \Delta\, v \qquad (13)$$

For the turbulent and the extreme load cases, the average values of electricity production will be obtained directly from ASHES to analyze instantaneous power under stochastic and extreme conditions.

Finally, it should be noted that the performance of a turbine in respect to AEP is assessed according to its Capacity Factor (C_p). C_p represents a ratio of the total annual energy production i.e. equivalent full load hours and the maximum possible energy production per year:

$$C_p = \frac{Annual\ Energy\ Production\ (kWh)}{Rated\ Power\ (kW) * 8760\ (h)} \qquad (14)$$

Chapter 4

Application of the methodology

4.1 Case study

The selected site for application of the methodology is UTSIRA NORD (Category A)[13]. It is located in the water depth between 185-280 m and 22 km from the south west Norwegian shore in the North Sea with the latitude 59.276˚ and longitude 4.541˚ (Figure 12). Norwegian continental shelf is characterized by deep waters, with high waves and complex seabed conditions. In 2013, the Norwegian Ministry of Petroleum and Energy commissioned Norwegian Water Resource and Energy Directorate (NVE) to assess environmental impact and opportunities for offshore wind development along Norwegian coast. NVE report showed that Utsira had one of the best wind resources of all 15 considered zones. The average wind speed is 10.2 m/s. The area covers 1010 km^2, which is heavily trafficked by freighters and shipping vessels. Closest populated zone is island of Utsira. In its Strategic Environmental Assessment report, NVE classified UTSIRA NORD as a priority offshore development site with the significant economic and technical conditions for development and grid integration by 2025 (NVE, 2013).

[13] Category A implies a priority zone for wind development as defined by Norwegian Water Resource Directorate report (2012).

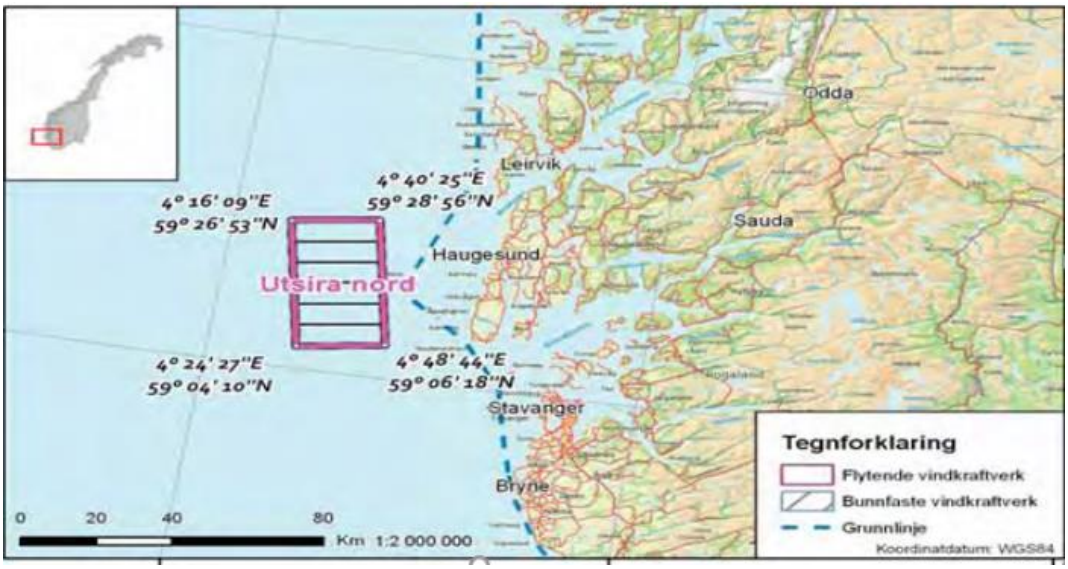

Figure 12: Location of development site UTSIRA NORD (NVE, 2012)

In 2017, NVE recommended to the Ministry of Petroleum and Energy to consider this site as one of the first potential demonstration sites for floating offshore development. Estimated capacity is between 500-1500 MW and the potential grid connection would be in Håvik (4COffshore, 2018). The latest announcements from the Norwegian government in August 2018 hinted that this could be one of two floating offshore sites designated for development in the upcoming period.

4.2 Sources of climatology data

In absence of real measurement data, the environmental conditions for UTSIRA NORD will be simulated based on the available online data, taking into account limitations associated with data averaging. The atmospheric conditions will be obtained from the Norwegian web portal *E-klima*[14] which gives free access to climatology database of the Norwegian Meteorological Institute. The closest station to UTSIRA NORD is "Utsira FYR 47300" (Figure 13), which will be taken as a meteorological station for reference values of wind speed and air temperature. Utsira FYR is located in Rogaland County, at latitude of 59.3065˚ and longitude of 4.8723˚ and is operational since 1860.

[14] www.eklima.met.no .

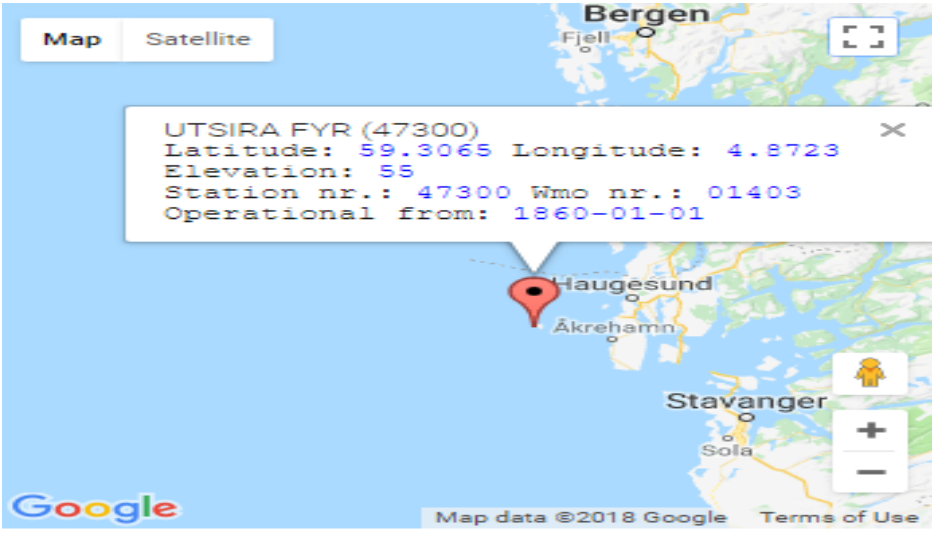

Figure 13: Location of weather station UTSIRA FYR 47300 (E-klima, 2018)

It is generally assumed that due to absence of physical obstacles and relatively low sea roughness in offshore conditions, there is an insignificant "horizontal spatial variation of long term mean wind speed" (Barthelmie, 2013 and Coelingh et al., 1996 as cited in Burton et al., 2011). Based on that, the long term mean wind speed data from Utsira FYR station will be applied to simulation site UTSIRA NORD. The wind speed and air temperature are obtained for 10-year (2008-2017) and air temperature for 30-year period (1961-1990) as shown in Appendix 4. The two periods are selected in order to reflect long-term (30 year) and medium-term environmental trends (10 year).

The same approach will be applied to sea temperature data. The online portal *E-klima* will be used to get sea temperature values for Gullfaks C (76923) located in the North Sea, which is the closest maritime weather station to UTSIRA NORD. Only 10-year values of sea temperature can be obtained from this station, since it operates from 1989. Sea temperature data for 30-year period will be assumed as average yearly sea values available from online portal *Sea Temperature*[15] for Utsira (Figure 14), which is based on several years of historically observed data.[16]

---

15 https://www.seatemperature.org/europe/norway/utsira.htm .

16 The portal does not mention the exact length of data observation.

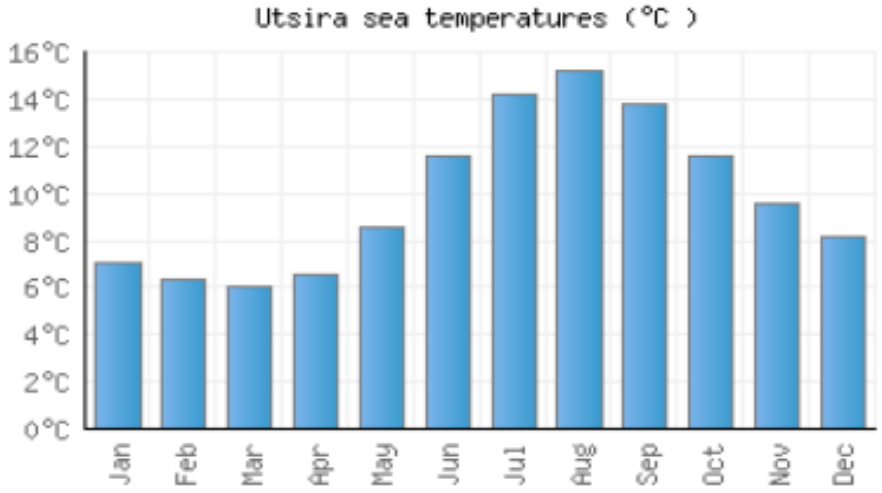

Figure 14: Average monthly sea temperatures at UTSIRA (SeaTemperature, 2018)

The values of significant wave height and wave period will be taken as referent values from the study "*Wave energy resource in the North Sea*" (Beels et al., 2007), which identified typical sea states in the North Sea for Belgian, Dutch, Norwegian, UK, Danish and German continental shelves. The reference site of Norwegian continental shelf under this study was Utsira. It was observed that significant wave height was larger than 1 m at this location for 80% of the time. The characteristic sea states with the significant wave height ($H_{s)}$ and wave energy period (T_e) for the Norwegian continental shelf are given in Table 1 based on study of Beels et al. (2007). Sea states are normally characterized by the significant wave height (H_s) and the mean wave period (T_m). However, it was argued that wave energy period, T_e[17] can better reflect the lower frequencies in energy variation in the wave spectrum than the mean wave period (Beels et al., 2007). Therefore, in the present analysis referent sea state with values of H_s and T_e will be used as per Table 1. Three sea states 1 (mild), 5 (mean) and 10 (rough or severe) are selected for modeling sea conditions in stepwise load cases LC1, LC2 and LC3, respectively.

[17] Defined as $Te = \frac{m-1}{m0}$, where m_n is the n^{th} moment of spectral density.

Table 1: Sea states on the Norwegian continental shelf (Beels et al., 2007)

Location		Utsira			
Mean water depth [m]		200			
Distance to shore [km]		21			
Average annual available wave power [kW/m]		23.12			
Sea State	1	2	3	4	5
H_s[m]	0.5	1.25	1.75	2.25	2.75
T_e[s]	7.13	7.44	7.69	8.04	8.39
Wave power [kW/m]	0.88	5.76	11.69	20.20	31.49
O.F.[%]	19.70	21.80	17.10	12.90	9.40
Sea State	6	7	8	9	10
H_s[m]	3.25	3.75	4.25	4.75	5.25
T_e[s]	8.80	9.01	9.09	9.51	9.96
Wave power [kW/m]	46.17	62.78	81.31	106.17	137.56
O.F.[%]	6.40	4.20	2.70	1.60	1.20

4.3 Input data for simulation

According to literature, there is a strong impact of the annual offshore cycle on the North Sea climatology, with the highest wind speeds occurring in winter and lowest in summer (Sušelj, Sood & Heinemann, 2009). Environmental conditions in load cases will be configured to reflect these temperature trends.

Default values for air and sea in ASHES are referenced to Standard Sea Level (SSL) conditions at 1 atm. For air conditions, at 15˚C air temperature, the air density is set to 1.225 kg/m^3 and dynamic viscosity at 1.81e-05kg/(m s). Default sea values are referenced to sea temperature at 10˚C, with average salinity of 3.5%, water density of 1,026.96 kg/m^3 and dynamic viscosity of 1.386e-03 kg/(m s). The mean water depth is 200 m. Wind and wave angles are kept at the default value of 0˚, assuming that the wind and wave angles are aligned. For all load cases, density and viscosity scheme of air and sea is calculated automatically by ASHES based on the input air and sea temperature and referenced to default values.

4.3.1 Input for stepwise wind

Under normal or stepwise wind option, the 3 load cases will be set up to model mild, mean (medium) and rough conditions, which can normally occur in the annual offshore

cycle in the North Sea. Each stepwise load case will run for 3650 s when it reaches cut-out wind speed of 25 m/s.

LC1 will represent “mild” case, with the summer air and sea temperatures taken for month of August, when the highest values are observed. Wave loads will be modeled according to Sea state 1. The air temperature will be taken from 30-year observation of the normal values for Utsira FYR and the sea temperature from the on-line portal *Sea Temperature* for August. Only one current will be modeled and hydro loads are enabled. Due to mild sea state we will assume no flow separation, hence, no wave or currents kinematic stretching will be modelled.

LC2 case will use the mean values from 10-year observations for air temperature at Utsira FYR and mean sea temperature from the *SeaTemperature* portal. The Sea state 5 will be used to represent medium sea state. This mean value is in line with the mean value of $H_s \approx 2.70$m obtained by 1990-2008 observations at Gullfaks C (Reistad et al., 2009). Also, the mean wind speed data agree well with Gullfaks C station (8 m/s) and Utsira FYR (8.1 m/s) measured at 10m height. Since the waves are moderate and 2 currents included, the Wheeler kinematic stretching is applied for both currents and wave modeling as well as hydro loads.

LC3 case will simulate rough met-ocean conditions, with air and sea temperature values typical for winter time, taken for month of February. The corresponding Sea state is 10, which represents the roughest characteristic sea state at Utsira. The air temperature will be taken from *E-klima* for 30 year period, with the lowest value in February and the sea temperature from the *Sea Temperature* portal for February. Wheeler kinematic stretching is applied for currents and waves as well as hydro loads.

4.3.2 Input for turbulent wind

For LC4 (NTM) we will assume mean environmental conditions (as in LC2), in combination with the mean Sea state 5. Since we will simulate mean met-ocean conditions, we will assume wind shear exponent as 0.14 (slightly lower than normal 0.2 to reflect milder conditions) and the normal sea surface roughness of 0.0002.

In LC5, the extreme turbulence wind file (ETM) will be used in conjunction with minimum values of air temperature (10-year period Utsira FYR observations), minimum sea temperature (10-year Gullfax C observations) and rough Sea state 10. Due to the rough sea, wind shear exponent is set to 0.2, with the sea roughness assumed as 0.0005 (which is slightly higher as compared to default 0.0002 in order to reflect higher waves).

For both turbulent load cases, the average wind speed at the rotor hub (90 m) was assumed as 12.6 m/s. Simulation will run 600 s, which is standard default length (Det Norske Veritas, 2013), with the random seed and horizontal and vertical flow angle of 0˚. Kinematic stretching will be applied only for waves. Under such a set up, it was not possible to add currents or hydro loads on tower, because the rotor moved outside turbulent wind field and simulation stopped.

4.3.3 Input for extreme wind

Extreme Wind Speed model (EWM) is selected as one of the IEC deterministic weather conditions available in ASHES for checking extreme load case (LC6). The reference mean wind speed at the hub height is 12.6 m/s, without shear and with default flow angle of 0˚. Air and sea temperature, and sea state conditions are modeled as in LC5, with extreme (minimum) values of air and sea over a 10-year period. The extreme event starts after 10 s and entire simulation runs for 600 s. Wheeler kinematic stretching is applied for both waves and currents and hydro loads on tower are enabled.

4.3.4 General simulation parameters

The general parameters can be set-up in ASHES under "*Analysis Parameter Dialogue*", to specify simulation type, ramp-up and convergence scheme, RPM, TSR, azimuth and pitch angle, aerodynamics and hydrodynamics.

General parameters are initially set up and have same values for all load cases (details are given in Appendix 3). The present work will be based on dynamic type of analysis, where behavior of real wind turbine is simulated using Newton's Second Law and elastic properties of the wind turbine to account for motion responses of the system. The rotor is modeled as flexible with all parts of RNA moving, where structural properties of blades

are drawn from geometry and stiffness of NREL 5 MW model (blade and airfoil properties), which can be additionally adjusted by using *Rotor* and *Blade* parameters. All time simulations have time step duration of 0.03 s as a default value assuming the rotor turns 2 degrees per one time step. Ramp-up scheme is dynamic, performed in time domain simulation and determined by time (duration), where loads are ramped-up from zero to their full value over a certain time (30 s default).

Convergence is achieved with a maximum number of iterations set to 1000. One time step can consist of a number of iterations which are repeated until the convergence is reached. Per each time step the total kinetic and total strain energy of the system is calculated. The new position of structure compared to the position of the structure in the previous time step is calculated with the equations of motion taking into account the forces applied to the structure. At each new position of the structure, the residual energy is obtained. If the ratio of residual energy over kinetic energy and the ratio of the residual energy over strain energy is bigger than the energy tolerances level, then a new position of the structure will be calculated and iteration repeated until the ratio is lower than the energy tolerances, after which the simulation moves to the next time step. If the convergence does not occur within 1000 iterations then the program would stop. In the simulations performed under current analysis, convergence usually occurred after 7 iterations under one time step. The number of iterations needed to complete one time step depends on the load case model, environmental parameters and tolerances selected.

For floating structures, due to relatively large motions, it is recommended to model aerodynamic and hydrodynamic loads as flexible in ASHES. Flexible modeling is achieved by computing velocity at current position and current time for air or wave particles as well as velocity of the structure at current time and position. RPM was set to 12, close to rated operating condition of the 5 MW NREL turbine (Liu et al., 2017). Simplified hydrodynamic model is adjusted by Morison's equation used in all sea states in a form of algorithm for perpendicular loading, defined by drag and inertia components and based on the water particle velocity and acceleration (ASHES, 2018).

Chapter 5

Results and discussion

In the following chapter, the main findings from the simulations will be presented and discussed.

5.1 AEP under stepwise wind

The AEP results for all three load cases show better electricity production of semi-submersible as compared to the spar in LC2 and LC3, albeit with a small difference (Table 2). Detailed results are presented in Appendix 5. The spar had highest energy yield under mild environmental conditions. With increase in environment loads, the semi-submersible floater slightly outperformed the spar. Under medium and extreme met-ocean conditions the structural responses of semi-submersible appear to have better capacity to dampen the system oscillations and resonances. It can be argued that such a small difference is attributed to use of the same baseline rotor and external controller properties of NREL 5 MW turbine, where torque was kept constant to limit the exaggeration in the power output. As pointed out in the literature, the pitch and heave motions have high impact on the platform motion affecting rotor aerodynamics, and consequently the power output. The relationship between platform pitch and heave motions and the power curve is further explained using results obtained under mean load case (LC2).

Table 2: AEP under stepwise wind in kWh

	Semi-submersible	Spar	Difference (%)
LC1	21 797 478.5	21 869 385.0	0.3
LC2	22 351 290.5	21 698 854.8	2.9
LC3	22 111 398.2	21 538 151.6	2.6

From Figure 15, it can be observed that both floaters under LC2 have similar power trend until entering the rated wind speed range (11-13 m/s), at which point the semi-submersible reaches rated power output before spar at the 12 m/s. Across the wind speed range of 8-13 m/s, the power output of semi-submersible is bigger than in the spar. In this range the energy density is the highest along the power curve, due to *k*-2 shaped Rayleigh annual frequency distribution, which combined with the higher power output gives slightly better yield to semi-submersible floater.

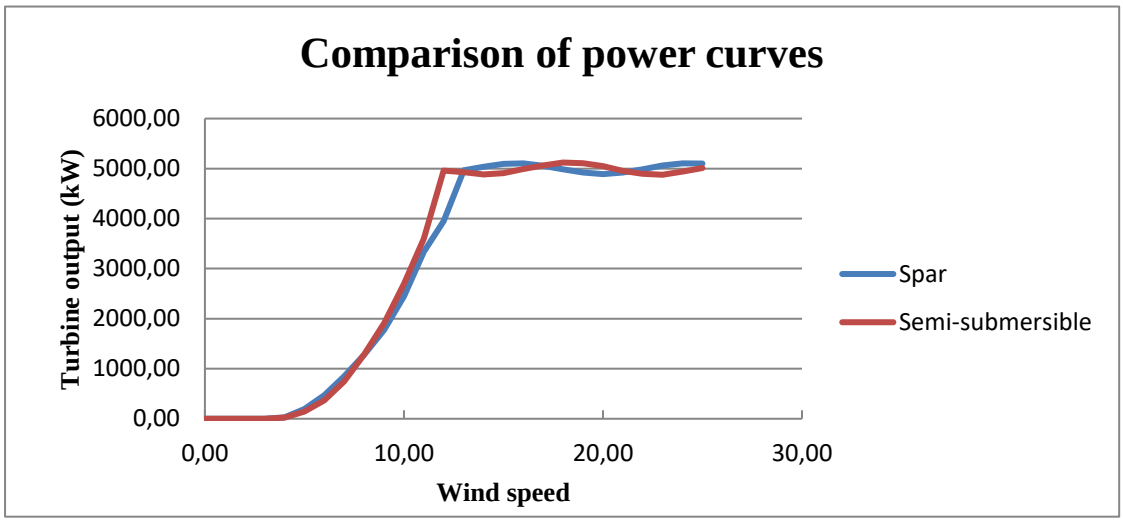

Figure 15: Comparison of power curves under LC2

Since both floaters use the same type of controller, a difference in electricity production can be attributed to the amplitude of floater's motion in pitch and heave modes. In the study of Bagbanci et al. (2015) pitch and heave motions were identified as the most

significant degrees of freedom that directly affect the power output. The values of pitch and heave per each wind speed change were plotted in Figure 16.

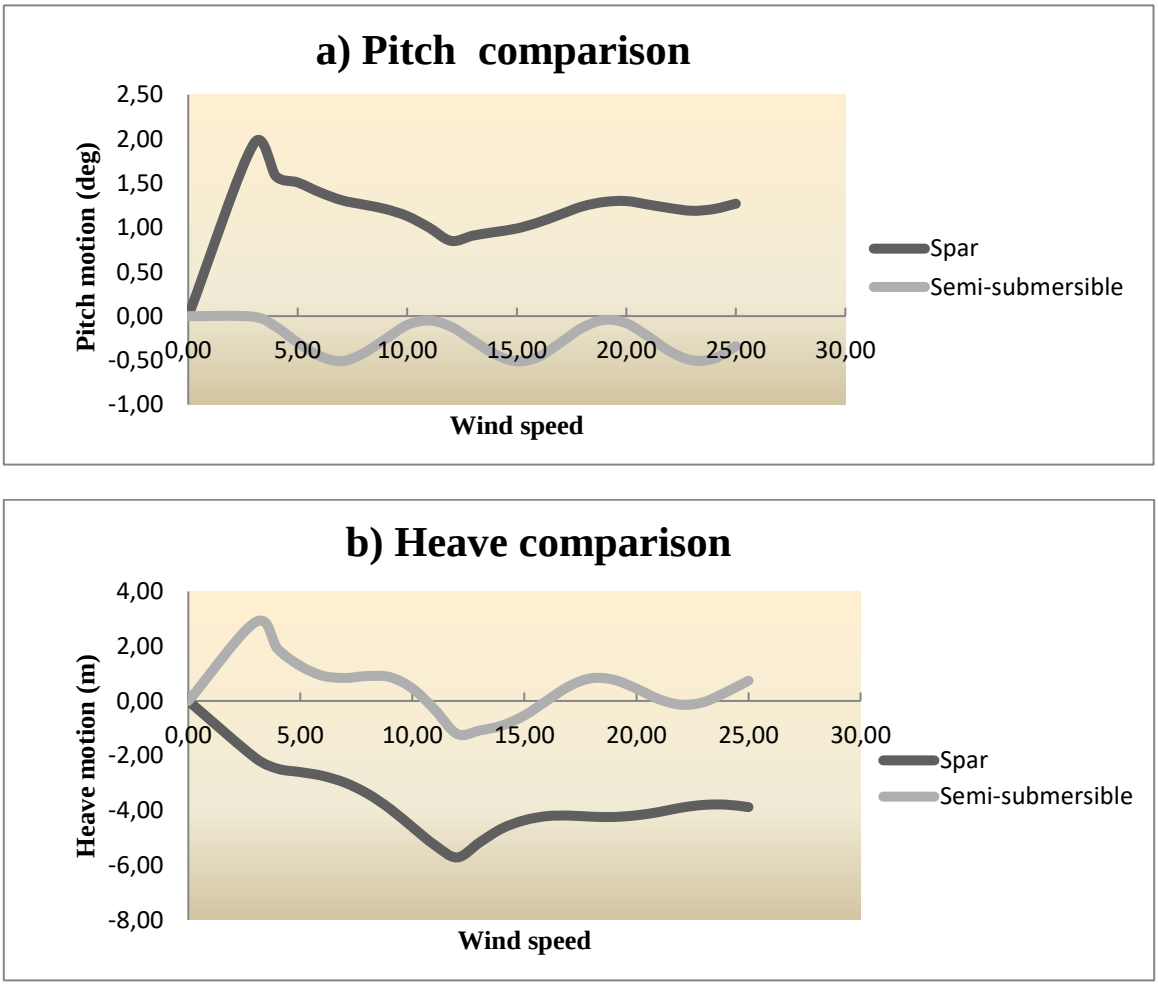

Figure 16: Comparison of pitch (a) and heave (b) motions under LC2

Around the rated operating range (11-13 m/s), both heave and pitch motions of the semi-submersible floater are smaller than in the spar and closer to zero (starting position when the floater is still and no wave forces are applied). It is assumed that due to water plain area and entrapment plates, the semi-submersible can sustain larger wave amplitudes as compared to spar whose draft diameter is smaller and more susceptible to bigger waves. In line with this argument, the spar performed better under LC1 at mild waves (0.3%) while under medium and more severe sea conditions semi-submersible was more stable

and generated better power output. Furthermore, it was observed that the hub displacement magnitude (Figure 17) is higher in the spar than semi-submersible with peaks for both floaters around 10 m/s, just before the turbine starts entering into operating range after which it slowly decreases. Larger amplitude motion of the spar in heave and pitch is translated to motion of the hub leading to its larger displacement. It is assumed that at some point, if there is bigger wave excitation force applied on spar floater which increases amplitude of its motion, the controller-response natural frequency might become bigger than platform – pitch natural frequency which would result in some loss of the energy where controller attempts to reduce negative damping to stabilize the power output.

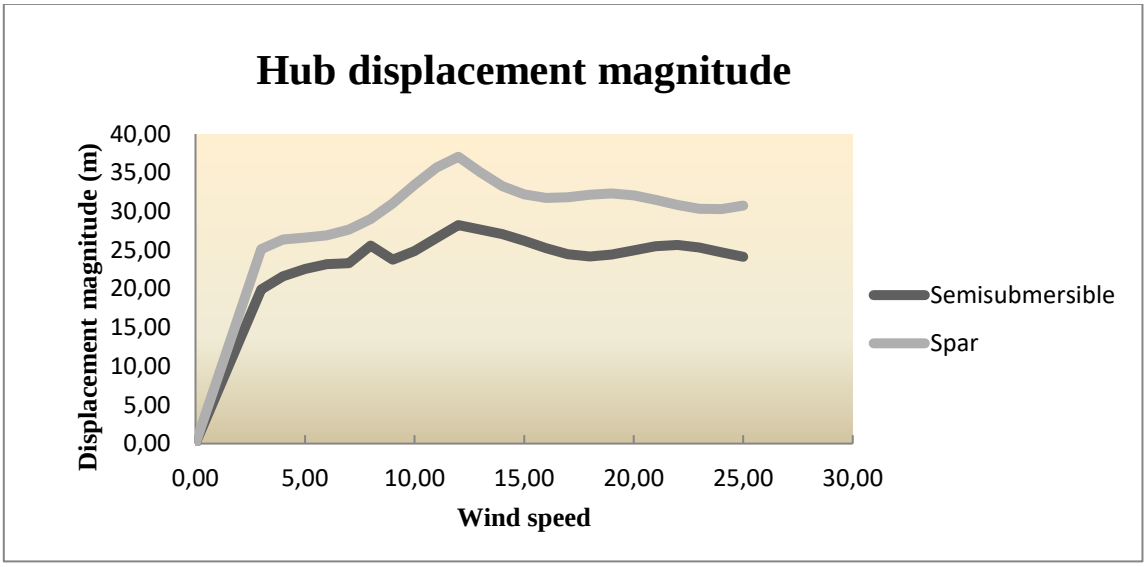

Figure 17: Comparison of hub displacement magnitude under LC2

Based on the above results, the smaller platform motion and bigger stability of the semi-submersible is apparently attributed to its geometrical properties:

- Larger mass and larger stability
- Water plane area stiffness bigger than in spar
- Buoyancy is larger than in spar
- Overall platform motion amplitude smaller than in spar

5.2 Power output under turbulent wind

The electricity production was taken as average output after removing first 120 s to avoid transient effects. The power output is almost same for both floaters under both turbulent load cases, with the negligible advantage of semi-submersible over spar (Table 3). In case of extreme turbulent wind and under extreme conditions, loads are bigger and the energy output smaller than under normal turbulent conditions.

Table 3: Average electricity production under turbulent wind in kWh

	Semi-submersible	**Spar**
LC4	490.65	489.34
LC5	476.46	476.41

Since the simulation was run only for 10 minutes, it was not possible to establish trends in respect to platform responses in pitch and heave motion and hub displacement magnitude. Secondly, it was not possible to simulate currents, currents kinematic stretching and hydro loads on the tower because rotor moved outside the turbulent grid and simulation stopped after around 30 seconds. Under such circumstances, it is assumed that the power output under both load cases might have been slightly exaggerated. Additional tests might be needed to better model turbulent load cases.

5.3 Power output under extreme wind

Average electricity output of floaters under IEC EWM extreme load case showed better performance of the semi-submersible than the spar, again with the very small difference (Table 4). Similarly as for turbulent load cases, the power results in first 120 s were not included in order to remove effects of rotor adjustment and power variation. The platform motion and hub displacements were not analyzed due to limited simulation time.

The average electricity production was bigger in both floaters under LC6 as compared to both turbulent load cases. This can be partly explained by the absence of stochastic effects and variations in wind speed and direction that may limit the power output. Another reason is that under extreme IEC load case the mean wind speed has been magnified which may have contributed to a higher electricity output.

Table 4: Average electricity production under extreme wind in kWh

	Semi-submersible	**Spar**
LC6	502.45	501.33

5.4 Sensitivity analysis

An important factor in any simulation is its length. What is a sufficient time for a generator to overcome the power overshooting and start simulating quite realistically the aerodynamic behavior of the rotor?

To answer this question, two sensitivity cases were compared under LC2:

- S1 with shorter time step difference (30 s for start-up and 15 s step difference)
- S2 with longer time step difference (500 for start –up and 300s step difference)

The results demonstrated the power overshoot in SC1 (23 422 299.5 kWh), which was almost 1 GWh bigger as compared to LC2 (22 351 290.5 kWh) and SC2 (22 311 710.9 kWh). When the time step difference in the simulation gets bigger, as in LC2 (2.5 min) and in SC2 (5 min), the transient effects of the rotor on the power are less powerful and the generator excursions above the rated power are smaller. Even though SC2 had twice as large time step duration than LC2, the power output exceeded 5 MW in 6 instances after the rated wind speed of 12 m/s was reached, as compared to LC2 which had 5 such instances. This showed that in ASHES the time step duration needs to be at least couple of minutes long (in our case 2.5 min) to get generally reliable results.

5.5 Summary

The results obtained from the simulation confirmed that the platform motion directly influences the field around rotor, its aerodynamic behavior and consequently, the power output. Overall, the semi-submersible had slightly better energy yield than the spar in all but one load case. The robustness of results was tested in the sensitivity analysis for the semi-submersible floater under LC2 in regards to the simulation length under stepwise wind module, which indicated that longer time steps of at least couple of minutes are needed to avoid power exaggeration.

Chapter 6

Conclusions

This study has investigated energy performance of the semi-submersible and the spar buoy floating wind turbines using aero-hydro-servo-elastic software ASHES.

In all six load cases, but one (LC1), the semi-submersible had slightly better energy yield than the spar. In particular, semi-submersible had best AEP under LC2, which is assumed as the most relevant study load case with the mean air and sea temperature and sea state conditions that prevail over the year at the case study site. Under the LC2, the actual difference in power curve is observed around rated operating range (11-13m/s), which the semi-submersible turbine enters before the spar with the higher power output. At the same wind speed range, heave and pitch motions of the semi-submersible are smaller than in the spar as well as hub displacement magnitude. It can be argued that specific geometric design with large plane area and entrapment plates of the semi-submersible improves the system stability and limits rotor displacements, which consequently benefits the power output.

Under LC2 the AEP difference was relatively small (2.9%), which may appear insignificant when we compare power output at the level of one turbine. However, even such a small difference in AEP is worth considering when planning a wind farm with installed capacity of few hundreds of MW because this difference can mean several millions in annual income which can affect investment decision which type of floater to use.

The floating wind turbines can sustain bigger loads up to certain level after which the electricity generation tends to decrease under more extreme climate conditions, which is evident from the results under stepwise wind. With increase in loads, power output of spar decreases in all load cases, and for semi-submersible it decreases from medium to more severe environment conditions. The appropriate modeling of hydro loads is extremely important in FOWT for an adequate representation of the floater-rotor interaction. The current analysis has used T_e (energy period of wave) for precise modeling of the characteristic sea state on the Norwegian continental shelf as compared to T_m (mean wave period) that is used in general analysis for any site, in order to better reflect lower frequencies in the wave energy.

As in any modeling process which is not confirmed by real test data, the current results should be treated as an approximation to physical behavior of the structure taking into consideration the modeling limitations. However, the most relevant features of the floating wind turbine system were modeled in ASHES, apart from aerodynamic effects of unsteady wind field which BEM cannot fully capture. Additionally, the currents and hydro loads on the tower proved to be hard to simulate under turbulent wind due to limitations in the grid refinement set-up.

The further research would ideally extend the findings from the present analysis to entire wind farm in order to analyze the impact of wake effects in the wind turbines placed in an array. A decision which floating offshore wind concept should be installed at a given site should be based not only on the electricity production but also taking into account a full range of financial factors, market conditions and regulatory framework. Therefore, it would be useful to complement this research by financial and investment analysis to assess the LCOE and profitability of different floating concepts, which might give a valuable insight in future deployment trends of the floating offshore wind technology for its optimal utilization.

REFERENCES

Al-Solihat, M.K. & Nahon, M. (2015) Mooring and hydrostatic restoring of offshore floating wind turbine platforms. *Oceans – St. St. John's, OCEANS 2014*. Available from: doi:10.1109/OCEANS.2014.7003269.

ASHES. (2018) *Technical Specifications*. Available from: https://www.simis.io/Products_Ashes_Technical-specifications [Accessed 20 July 2018]

Bagbanci H., Karmakar D. & Soares G.C. (2015) Comparison of spar and semisubmersible floater concepts of offshore wind turbines using long-term analysis. *Journal of Offshore Mechanics and Arctic Engineering*. Available from: doi:137. 10.1115/1.4031312.

Beels, C., Henriques, J.C.C., De Rouck, J., Pontes, M.T., De Backer, G. & Verhaeghe H. (2007) Wave energy resource in the North Sea. *European Wave and Tidal Energy Conference Series.* Available from: doi:10.13140/2.1.4640.6403.

British Standard Institution (2006) *BS-EN 61400-1:2005. Wind turbines - Part 1: Design requirements (IEC 61400-1:2005)*. London, BSI

British Standard Institution (2009) *BS-EN 61400-3:2009. Wind turbines - Part 3: Design requirements for offshore wind turbines (IEC 61400-3:2009)*. London, BSI

Butterfield S., Musial, W., Jonkman, J.& Sclavounos, P. (2007) Engineering challenges for floating offshore wind turbines. In: NREL/CP-500-38776, *Conference Paper: Copenhagen Offshore Wind Conference Copenhagen, Denmark October 26–28, 2005* Available from: https://www.nrel.gov/docs/fy07osti/38776.pdf [Accessed 20 June 2018]

Burton, T., Jenkins, N., Sharpe, D. & Bossanyi, E. (2011) *Wind energy handbook*. Chichester: Wiley & Sons, Ltd.

Carbon Trust (2015) *Floating offshore wind: Market and technology review*. Available from:https://www.carbontrust.com/media/670664/floating-offshore-wind-market-technology-review.pdf [Accessed 17 June 2018]

Danish Wind Industry Association. (2003) *Offshore wind conditions.* Available from: http://xn--drmstrre-64ad.dk/wp-content/wind/miller/windpower%20web/en/tour/wres/offshore.htm [Accessed 15 August 2018]

Deign, J. (2018) Norway advances in the flaoting offshore wind race. *Greentech Media*. Avaiable from: https://www.greentechmedia.com/articles/read/norway-advances-in-floating-offshore-wind-race#gs.qSDUL9Y [Accessed 26 August 2018]

Det Norske Veritas (2010) *Recommended practice DNV-RP-C2015. Environmental conditions and environmental loads*. DNV AS

Det Norske Veritas (2013) *Offshore standard DNV-OS-J103. Design of floating wind turbine structures*. DNV AS

Det Norske Veritas (2014) *Offshore standard DNV –OS-J101. Design of offshore wind turbine structures*. DNV AS

E-klima. (2018) E-klima Home Page. Available from: http://sharki.oslo.dnmi.no/portal/page?_pageid=73,39035,73_39049&_dad=portal&_schema=PORTAL [Accessed 17 August 2018]

Equinor. (2018) *Hywind- the world's leading floating offshore wind solution*. Available from: https://www.equinor.com/en/what-we-do/hywind-where-the-wind-takes-us.html [Accessed 28 August 2018]

European Commission. (2011) *Energy roadmap 2011*. Available from: https://eur-lex.europa.eu/legal-content/EN/ALL/?uri=CELEX:52011DC0885 [Accessed 18 June 2018]

EWEA. (2013) *Deep water. The next step for offshore wind energy*. Available from: http://www.ewea.org/fileadmin/files/library/publications/reports/Deep_Water.pdf [Accessed 20 August 2018]

4COffshore. (2018) *Utsira Nord (Category A area) offshore wind farm*. Available from:https://www.4coffshore.com/windfarms/Utsira-nord-Norway-NO44.html [Accessed 22 August 2018]

Goupee, A.J., Kimball, R.W. & Dagher, H.J. (2016) Experimental observations of active blade pitch and generator control influence on floating wind turbine response. *Journal of Renewable Energy*. Vol. 104, pp. 9-19

Hau, E. (2013) *Wind turbines, fundamentals, technologies, application, economics*. Berlin-Heidelberg: Springer-Verlag

Henderson, A.R. (2009) *Offshore wind energy in deep waters*. In: Twidell J. & Gaudiosi G. ed. *Offshore Wind Power*. Essex: Multi Science Publishing Co. Ltd.

Jeon , M.,Lee, S. & Lee, S. (2014) Unsteady aerodynamics of offshore floating wind turbines in platform pitching motion using vortex lattice method. *Journal of Renewable Energy*. Vol. 65, pp. 207-212. Available from: doi:10.1016/j.renene.2013.09.009.

Jonkman, J. (2010) *Definition of the floating system for Phase IV of OC3*. NREL. Technical report: NREL/TP-500-47535. Available from: https://www.nrel.gov/docs/fy10osti/47535.pdf. [Accessed 11 August 2018]

Jonkman, J. (2010) *Definition of the floating system for Phase IV of OC3*. NREL. Technical report: NREL/TP-500-47535. Available from: https://www.nrel.gov/docs/fy10osti/47535.pdf. [Accessed 11 August 2018]

Jonkman, J. (2013) The new modularization framework for the FAST wind turbine CAE tool. In: NREL/CP-5000-57228 *Conference Paper*: *To be presented at the 51st AIAA Aerospace Sciences Meeting, including the New Horizons Forum and Aerospace Exposition Dallas, Texas January 7-10, 2013*. Available from: https://www.nrel.gov/docs/fy13osti/57228.pdf. [Accessed 12 August 2018]

Kelley, N.D. & Jonkman, B.J. (2007) *Overview of TurbSim stochastic inflow turbulence simulator*. *Version 1.21*. NREL. Technical report: NREL/TP-500-41137. Available from: https://nwtc.nrel.gov/system/files/TurbSimOverview.pdf [Accessed 15 August 2018]

Krogstad, P.A. & Eriksen, P.E. (2011) *Blind test workshop calculations for a model wind turbine. Summary report*. Trondheim: NTNU.

Lin, L., Wang. K. & Vassalos, D. (2018) Detecting wake performance of floating offshore wind turbine. *Journal of Ocean Engineering*. Vol. 156, pp. 263-276.

Liu, Y., Xiao, Q., Incecik, A. & Wan, D. (2015) Investigation of the effects of platform motion on the aerodynamics of a floating offshore wind turbine. *Journal of Hydrodynamics*. Vol. 28(1), pp. 95-101.

Liu, Y., Xiao, Q., Incecik, A., Peyrard, C. & Wan, D. (2017) Establishing a fully coupled CFD analysis tool for floating offshore wind turbines. *Journal of Renewable Energy*. Vol. 112, pp. 280-301.

Liu, Y., Li, S., Yi, Q. And Chen, D. (2016) Developments in semi-submersible sloating foundations supporting wind turbines: A Comprehensive Review. *Journal of Renewable and Sustainable Energy Reviews*. Vol. 60, pp. 413-449.

Longbin T. & Shunqing C. (2004) *Heave motion suppression of a spar with a heave plate*. Available from: https://researchrepository.griffith.edu.au/bitstream/handle/10072/21561/30784_1.pdf?sequence=2 [Accessed 24 July 2018]

Ma, Y., Sclavounos, P.D., Whiter, J.C. & Arora, D. (2018) Wave forecast and its application to the optimal control of offshore floating wind turbine for load mitigation. *Journal of Renewable Energy*. Vol. 128, pp. 163-176.

Manwell, J.F., McGowan, J.G. & Rogers, A.L. (2009) *Wind Energy Explained. Theory, Design and Application*. Chichester: Wiley & Sons Ltd.

Moriarty, P.J. & Hansen, A.C. (2015) *AeroDyn Theory Manual*. NREL. Technical report: NREL/TP-500-36881. Available from: https://www.nrel.gov/docs/fy05osti/36881.pdf [Accessed 7 September 2018]

NVE. (2012) *NVE-Rapport 47-12, Havvind – Strategisk Konsekvensutredning*. Norges vassdrags- og energidirektorat. Available from: http://publikasjoner.nve.no/rapport/2012/rapport2012_47.pdf [Accessed 8 September 2018]

NVE. (2013) *Offshore wind power in Norway: Strategic Environmental Assessment (English Summary)*. Norwegian Water Resource and Energy Directorate. Available from: http://publikasjoner.nve.no/diverse/2013/havvindsummary2013.pdf [Accessed 4 August 2018]

Plumley, C., Leithead, W., Jamieson, P., Bossanyi, E., Graham, M. (2014) Comparison of Individual Pitch and Smart Rotor Control Strategies for Load Reduction. *Journal of Physics: Conference Series*. Vol. 524 – 012054

Popko, W., Huhn, M.L., Robertson, A., Jonkman, J., Wendt, F., Müller, K.,... Pengchang, F. (2018) Verification of a numerical model of the offshore wind turbine from the Alpha Ventus Wind Farm within OC5 Phase 3. Conference paper OMAE2018-77589. *Conference paper: The 37th International Conference on Ocean, Offshore and Arctic Engineering OMAE 2018, Madrid.* Available from: https://www.researchgate.net/publication/326294528_Verification_of_a_Numerical_Model_of_the_Offshore_Wind_Turbine_from_the_Alpha_Ventus_Wind_Farm_within_OC5_Phase_III [Accessed 21 August 2018]

Reistad, M., Brevik, Ø., Haakestand, H., Aarnes, O.J. & Furevisk, B.R. (2009) *A high resolution hindcast of wind and waves for the North sea, the Norwegian Sea and the Berents Sea*. Norwegian Meteorological Institute. Report No. 2009/14. Available from: file:///C:/Users/Samsung/Downloads/MET-report-14-2009%20(2).pdf [Accessed 20 July 2018]

Robertson, A., Jonkman, J., Masciola, M., Song, H., Goupee, A., Coulling, A. & Luan, C. (2014) *Definition of the Semi-Submersible Floating System for Phase II of OC4*. NREL. Technical report: NREL/TP-5000-60601. Available from: https://www.nrel.gov/docs/fy14osti/60601.pdf [Accessed 12 August 2018]

SeaTemperature. (2018) *Utsira sea temperature*. Available from: https://www.seatemperature.org/europe/norway/utsira.htm [Accessed 20 August 2018]

Shen, X., Chen, J., Hu, P. Zhu, X. & Du, Z. (2018) Study of the unsteady aerodynamics of floating wind turbines. *Journal of Energy*. Vol. 145, pp.783-809.

Simscale. (2018) *Finite Element Method- What is it? FEM and FEA explained*. Available from: https://www.simscale.com/blog/2016/10/what-is-finite-element-method/ [Accessed 28 June 2018)

Sušelj, K., Sood, A. & Heinemann, D. (2009) North Sea near surface wind climate and its relation to the large scale circulation patterns. *Theoretical and Applied Climatology*. (2010) 99:403–419. Available from: doi:10.1007/s00704-009-0149-2.

Thomassen, P., Bruheim, P.J., Suja, L. & Frøyd L. (2012) A novel tool for FEM analysis of offshore wind turbines with innovative visualization effects. In: International Society of Offshore and Polar Engineers, 2012. *Proceedings of the Twenty-second (2012) International Offshore and Polar Engineering Conference, Rhodes, Greece, June 17–22, 2012*.

Tran, T.T. & Kim, D.H. (2015) The Platform pitching Motion of Floating Offshore Wind Turbine: A Preliminary Unsteady Aerodynamic Analysis. *Journal of Wind Engineering and Industrial Aerodynamics*. Vol. 142, pp. 65-81.

Türk. M. & Emeis, S. (2010) The dependence of offshore turbulence intensity on wind speed. *Journal of Wind Engineering and Industrial Aerodynamics*. Vol. 98, pp. 466-471. Available from: doi:10.1016/j.jweia.2010.02.005.

Wauki, T., Yoshimura, M. & Yokoyama, R. (2017) Multiple-feedback control of power output and platform pitching motion for a floating offshore wind turbine-generator system. *Journal of Energy*. Vol. 141, pp. 563-578.

WIND EUROPE. (2017) *Floating offshore wind vision statement*. Available from: https://windeurope.org/wp-content/uploads/files/about-wind/reports/Floating-offshore-statement.pdf [Accessed 18 June 2018]

WIND EUROPE. (2017) *Wind in power 2017*. Available from: https://windeurope.org/wp-content/uploads/files/about-wind/statistics/WindEurope-Annual-Statistics-2017.pdf [Accessed 18 June 2018]

APPENDIX 1: INPUT PARAMETERS FOR LOAD CASES

Parameter	*Load case 1*	*Load case 2*	*Load case 3*	*Load case 4*	*Load case 5*	*Load case 6*
Wind type	Stepwise (Mild)	Stepwise (Mean)	Stepwise (Rough)	Turbulent (Mean)	Turbulent (Extreme)	IEC EWM (Extreme)
Air (˚C)	13.6	8.4	1.7	8.4	-6.5	-6.5
Sea (˚C)	15	10	6	10	0	0
H_s (m)	0.5	2.75	5.25	2.75	5.25	5.25
T_e (s)	7.13	8.39	9.96	8.39	9.96	9.96
Sea state	1	5	10	5	10	10
Currents	1	2	2	None	None	2
Wave kinematic stretching	None	Yes (Wheeler)	Yes (Wheeler)	Yes (Wheeler)	Yes (Wheeler)	Yes (Wheeler)
Currents kinematic stretching	None	Yes (Wheeler)	Yes (Wheeler)	No	No	Yes (Wheeler)
Tubular tower hydro loading	Yes	Yes	Yes	No	No	Yes

APPENDIX 2: WIND FILE DATA

a) Stepwise wind file used for LC1, LC2 and LC3

```
# This text file represents a stepwise wind history that can be imported into Ashes.
# i.e. the wind is constant between step changes.
# windspeed is positive downwind.
# windangle is relative to North (i.e. the y axis). Thus, it is positive when coming from the north - east.
# (by default the wind turbine faces North)
#
# time   windspeed   windangle
0     0   0
300   3   0
500   4   0
650   5   0
800   6   0
950   7   0
1100  8   0
1250  9   0
1400  10  0
1550  11  0
1700  12  0
1850  13  0
2000  14  0
2150  15  0
2300  16  0
2450  17  0
2600  18  0
2750  19  0
2900  20  0
3050  21  0
3200  22  0
3350  23  0
3500  24  0
3650  25  0
3800   0  0
```

b) Turbulent wind files used for LC4 and LC5

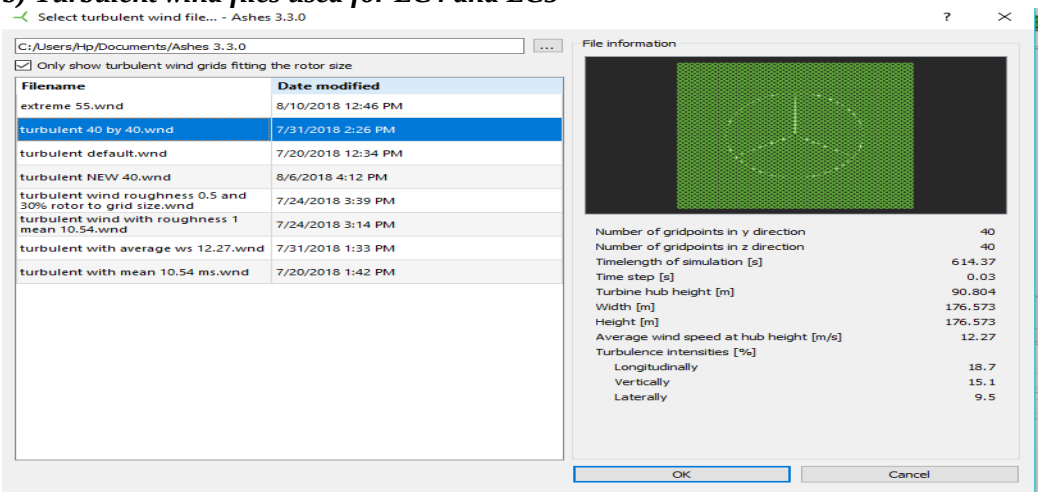

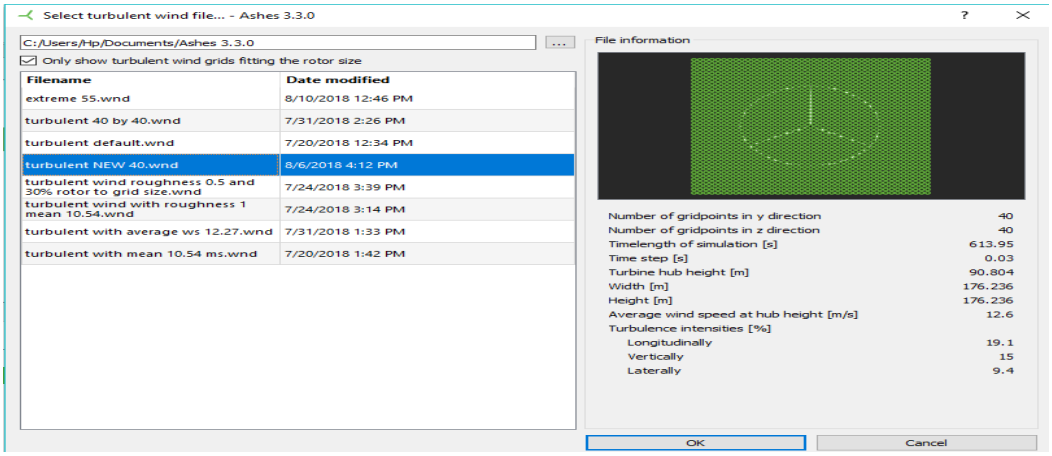

APPENDIX 3: SIMULATION DATA

a) Baseline properties of OC4 semi-submersible floater used in ASHES

Platform total mass (including ballast):	13,473t		
Height:	30 m	Offset columns:	3
Base elevation:	-19.196 m	Distance:	28.87 m
Top elevation:	10.804 m	Upper diameter:	12 m
Material:	SteelUndamped	Upper thickness:	0.06 m
Modulus of elasticity:	2.1e+11 N/m^2	CM location below SWL:	13.46 m
Max buoyancy:	171,458 kN	Platform roll inertia about CM:	6.827E+9 kg/m^2
Center of buoyancy below SWL:	13.15 m	Platform pitch inertia about CM:	6.827E+9 kg/m^2
Draft (initial):	19.196 m	Platform yaw inertia about CM:	1.226E+10 kg/m^2
Total water plane area stiffness:	3,812.0 kN/m	Center of buoyancy below SWL:	13.15 m
Main column Diameter:	6.5 m		
Main column Thickness:	0.03 m		

b) Baseline properties of OC3 spar floater used in ASHES

Platform total mass (including ballast):	7,466.0t	Upper diameter:	6.5 m
Height:	130 m	Upper thickness:	0.05 m
Base elevation:	-120 m	Lower diameter:	9.4 m
Top elevation:	10 m	Lower thickness:	0.05 m
Material:	SteelRayDamped	CM location below SWL:	89.9 m
Modulus of elasticity:	2.1e+11 N/m^2	CG below SWL:	75 m
Max buoyancy:	84,293 kN	Platform roll inertia about CM:	4229.23E6 $kg\text{-}m^2$
Draft (initial):	120 m	Platform pitch inertia about CM:	4229.23E6 $kg\text{-}m^2$
Total water plane area stiffness:	334.2 kN/m	Platform yaw inertia about CM:	164.23E6 $kg\text{-}m^2$

c) Fundamental properties of the 5 MW NREL used in ASHES

Rotor position:	Horizontal axis
Rotor orientation:	Upwind, 3 blades
Rating:	5 MW
Control:	External controller OC3 PhaseIV
RNA mass:	350,000 kg
Drive train:	High speed, multiple state
Rotor hub diameter:	125.9 m
Rotor swept area:	12,446 m^2
Hub height :	90.804 m
Cut –in, rated, cut out wind speed:	3, 11.5, 25
Transmission system:	Geared
Rotor tilt angle:	5
Cone angle:	2.5
Brake location:	Low speed shaft
Rated tip speed:	80 m/s

d) Overview of general analysis parameters used in ASHES

Analysis type:	Dynamic
Rotor model:	Flexible
Timestep scheme:	Calculated (0.03 s default)
Load ramp-up scheme:	Duration
Analysis type for ramp-up:	Dynamic
Convergence (max. iterations):	1000 (default)
Analysis mode:	Non-linear solver
Aerodynamic movement of structure:	Flexible
Hub loss correction:	Enabled
Tip loss correction:	Enabled (Prandlt)
Critical Glauert's value:	0.33
RPM:	12
Tower shadow:	Enabled
Hydrodynamic movement of structure:	Flexible
Algorithm for perpendicular loading (hydro):	Morison
Moving structure for perpendicular drag (hydro):	Moving
Moving structure for perpendicular inertia (hydro):	Moving
Hydro loads below seabed:	Enabled

e) Default properties of semi-submersible floater

Number of mooring lines	3
Angle between lines	120˚
Type of anchoring	Catenary
Line diameter	0.0766
Anchor distance	853.87 m
Fairlead center distance	12 m
Mooring line distributed mass	113.35 kg/m
Elastic modulus	1.8975e+11 Pa
Yaw spring stiffness	3.278e+06 N m/rad

f) Default properties of spar floater

Number of mooring lines	3
Angle between lines	120˚
Type of anchoring	Catenary
Line diameter	0.09
Anchor distance	853.87 m
Fairlead center distance	4.7 m
Mooring line distributed mass	77.7 kg/m
Elastic modulus	1.8975e+11 Pa
Yaw spring stiffness	3.278e+06 N m/rad

APPENDIX 4: CLIMATE DATA

a) 10-year wind data and wind rose at Utsira FYR (e-Klima report, 2018)

FREQUENCY DISTRIBUTION - WIND ROSE

Stations

Stnr	Name	Operates from	Operates until	Altitude	Latitude	Longitude	Municipality	County	Region
47300	UTSIRA FYR	Jan 1860		55	59,3065	4,8723	Utsira	Rogaland	WESTERN NORWAY

Elements

Code	Name	Unit
DD	Wind direction (FF)	degrees
FF	Wind speed (10 meters above ground)	m/s

Norwegian Mean Time (NMT) is the same as Central European Time which is the timezone one hour before UTC, and is therefore often describ

********** NOTE **********

In the period 01.01.2008 - 31.12.2017 data from the hourly observations are used for FF and DD.

****

47300 Relative frequencies (%) of observations grouped by DD horizontally and FF vertically. 01.01.2008 - 31.12.2017

All available months. All available hours

DD	345 - 15	15 - 45	45 - 75	75 - 105	105 - 135	135 - 165	165 - 195	195 - 225	225 - 255	255 - 285	285 - 315	315 - 345	Variable	Calm	Total	Rel.fr.	Cum.fr.	Mean DD	St.dev. DD
FF	14	44	74	104	134	164	194	224	254	284	314	344							
<= 0,2														0,8	683	0,8	0,8		
0,3 - 7,7	5,2	3,5	2,3	3,3	5,2	5,2	5,7	4,8	4,0	3,8	3,8	4,6			42031	51,5	52,3		
7,8 - 15,2	5,0	0,7	0,2	0,9	3,7	5,8	6,8	3,8	3,3	3,4	2,6	4,4	0,0		33104	40,6	92,9		
15,3 - 22,7	0,8	0,0	0,0	0,0	0,6	1,5	0,9	0,4	0,5	0,8	0,5	0,7			5572	6,8	99,7		
22,8 - 30,2	0,0				0,0	0,1	0,0	0,0	0,0	0,0	0,0	0,0			205	0,3	100,0		
> 30,2	0,0									0,0	0,0				4	0,0	100,0		
Total	8983	3458	2092	3414	7714	10297	10916	7410	6449	6636	5599	7947	1	683	81599				
Rel.fr.	11,0	4,2	2,6	4,2	9,5	12,6	13,4	9,1	7,9	8,1	6,9	9,7	0,0	0,8		100,0			
Cum.fr.	11,0	15,2	17,8	22,0	31,4	44,1	57,4	66,5	74,4	82,6	89,4	99,2	99,2	100,0					
Mean FF	8,7	5,5	4,2	5,4	7,8	9,4	8,8	7,9	8,3	8,8	7,9	8,6	11,9	0,0					
St.dev. FF	4,2	2,9	2,3	3,1	4,1	4,7	4,0	4,0	4,4	4,7	4,5	4,3		0,1					

Statistics

Statistics	FF	DD	Date
Mean	8,1		
St.dev.	4,4		
Min FF	0,0		03.05.2008 21:00
Max FF	31,9		19.01.2008 03:00
Min DD			
Max DD			
Data coverage	93%	93%	

Time of observations are given in Norwegian Mean Time (NMT=UTC+1)

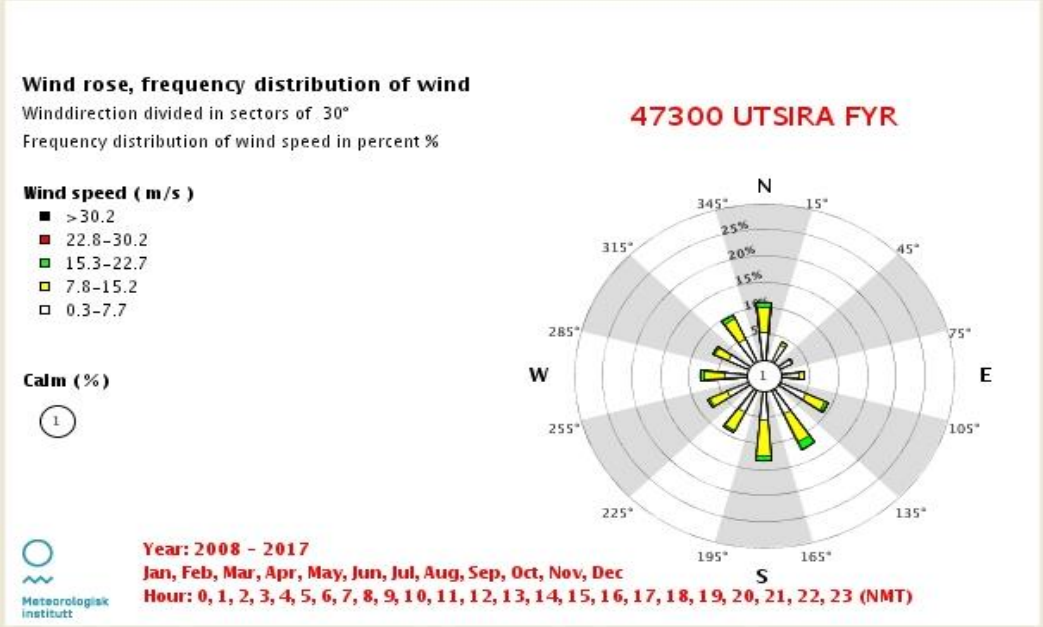

b) 10 year mean values at Utsira FYR (e-Klima, 2018)

Monthly values per element, with summaries Norwegian Meteorological Institute

Stations

Stnr	Name	Operates from	Operates until	Altitude	Latitude	Longitude	Municipality	County	Region
47300	UTSIRA FYR	Jan 1860		55	59,3065	4,8723	Utsira	Rogaland	WESTERN NORWAY

47300 UTSIRA FYR, Mean temperature (TAM)

Year	Jan	Feb	Mar	Apr	May	Jun	Jul	Aug	Sep	Oct	Nov	Dec	Total	Mean	Normal	Deviation	%
2008	4,4	4,9	3,4	6,3	10,2	13,0	16,6	15,6	13,1	9,3	6,3	4,5		9,0	7,4	1,6	
2009	3,4	1,4	4,2	7,1	9,5	12,3	15,8	15,1	13,0	8,6	7,5	2,7		8,4	7,4	1,0	
2010	-0,6	-0,2	3,6	5,8	7,6	10,7	14,2	15,0	12,6	9,1	2,9	-0,4		6,7	7,4	-0,7	
2011	2,6	0,7	2,5	6,7	9,3	11,6	14,1	14,8	12,9	10,2	8,7	5,0		8,3	7,4	0,9	
2012	3,5	2,8	5,1	5,0	8,5	10,8	13,6	15,1	11,6	8,3	7,0	1,6		7,7	7,4	0,3	
2013	1,4	0,8	0,8	4,5	9,2	12,0	14,3	15,2	13,0	10,4	7,0	6,5		7,9	7,4	0,5	
2014	3,0	4,6	5,3	7,5	9,6	12,8	17,1	15,1	14,2	11,2	8,4	5,4		9,5	7,4	2,1	
2015	4,6	4,3	5,0	5,5	7,8	10,4	12,9	15,7	13,5	10,7	8,1	6,8		8,8	7,4	1,4	
2016	2,3	3,3	4,0	5,7	10,0	13,0	14,3	14,0	15,3	9,9	5,6	6,9		8,7	7,4	1,3	
2017	4,8	3,4	4,5	5,8	9,5	12,2	13,7	14,4	13,7	10,7	6,7	4,9		8,7	7,4	1,3	
Number of	10	10	10	10	10	10	10	10	10	10	10	10					
Minimum	-0,6	-0,2	0,8	4,5	7,6	10,4	12,9	14,0	11,6	8,3	2,9	-0,4					
Year	2010	2010	2013	2013	2010	2015	2015	2016	2012	2012	2010	2010					
Maximum	4,8	4,9	5,3	7,5	10,2	13,0	17,1	15,7	15,3	11,2	8,7	6,9					
Year	2017	2008	2014	2014	2008	2008	2014	2015	2016	2014	2011	2016					
Total																	
Mean	2,9	2,6	3,8	6,0	9,1	11,9	14,7	15,0	13,3	9,8	6,8	4,4					
Normal	2,3	1,7	2,7	4,6	8,3	11,4	13,0	13,6	11,7	9,3	5,9	3,9					

c) 30-year normal air temperature values at Utsira FYR (e-Klima, 2018)

Monthly normal values Norwegian Meteorological Institute

Stations

Stnr	Name	Operates from	Operates until	Altitude	Latitude	Longitude	Municipality	County	Region
47300	UTSIRA FYR	Jan 1860		55	59,3065	4,8723	Utsira	Rogaland	WESTERN NORWAY

Month normals 1961 - 1990 for TAM, Mean temperature

St.no	Jan	Feb	Mar	Apr	May	Jun	Jul	Aug	Sep	Oct	Nov	Dec	Year
47300	2,3	1,7	2,7	4,6	8,3	11,4	13,0	13,6	11,7	9,3	5,9	3,9	7,4

APPENDIX 5: AEP RESULTS

LC1: Semi-submersible

Variable	Value	Unit
Mean velocity	10,20	m/s
Nominal power	5000	kW
Scale factor	11,51	m/s
Maximum energy yield	43800000	kWh
Capacity factor	0,498	-

Wind speed	Rayleigh distribution of yearly hours	Power curve	Energy yield kWh
0	0	0	0
1	131,2638535	0	0
2	256,6490587	0	0
3	370,7135714	0	0
4	468,8433849	35	16409,51847
5	547,5595989	176,4	96589,51325
6	604,7129288	402,2	243215,5399
7	639,5517254	726	464570,3733
8	652,6649246	1168,5	762638,9643
9	645,8155054	1747,2	1128368,851
10	621,6911003	2492,4	1549502,898
11	583,6050588	3428,5	2000889,944
12	535,1830388	4475,7	2395318,727
13	480,0673832	5004,8	2402641,239
14	421,6650992	4996,3	2106765,335
15	362,9565789	4995,8	1813258,477
16	306,3728029	4999,6	1531741,465
17	253,7400271	5007,5	1270603,186
18	206,2839408	5001,1	1031646,616
19	164,6805805	5012,1	825395,5376
20	129,139077	5005,1	646353,9945
21	99,50133132	5017,2	499218,0795
22	75,34548145	5007,2	377269,8947
23	56,08288189	5020,2	281547,2837
24	41,04163966	5009,1	205581,6772
25	29,53299319	5009,7	147951,436
26	20,89959258	0	0
27	14,54682693	0	0
28	9,959684816	0	0
29	6,708287045	0	0
30	4,445329839	0	0
		Total	21797478,55

LC1: Spar-buoy

Variable	Value	Unit
Mean velocity	10,20	m/s
Nominal power	5000	kW
Scale factor	11,51	m/s
Maximum energy yield	43800000	kWh
Capacity factor	0,499	-

Wind speed	Rayleigh distribution of yearly hours	Power curve	Energy yield kWh
0	0	0	0
1	131,2638535	0	0
2	256,6490587	0	0
3	370,7135714	0	0
4	468,8433849	36,5	17112,78355
5	547,5595989	181,3	99272,55528
6	604,7129288	412,1	249202,1979
7	639,5517254	741	473907,8285
8	652,6649246	1190,1	776736,5267
9	645,8155054	1762,4	1138185,247
10	621,6911003	2515,1	1563615,286
11	583,6050588	3453,7	2015596,792
12	535,1830388	4532,3	2425610,087
13	480,0673832	4991,8	2396400,363
14	421,6650992	4991,8	2104867,842
15	362,9565789	4992	1811879,242
16	306,3728029	4994,6	1530209,601
17	253,7400271	4985,5	1265020,905
18	206,2839408	4990,2	1029398,121
19	164,6805805	4984,2	820800,9494
20	129,139077	4992,3	644701,0143
21	99,50133132	4989,5	496461,8926
22	75,34548145	4999,5	376689,7345
23	56,08288189	4997,6	280279,8106
24	41,04163966	5008,9	205573,4689
25	29,53299319	5006,7	147862,837
26	20,89959258	0	0
27	14,54682693	0	0
28	9,959684816	0	0
29	6,708287045	0	0
30	4,445329839	0	0
		Total	21869385,09

LC2: Semi-submersible

Variable	Value	Unit
Mean velocity	10,20	m/s
Nominal power	5000	kW
Scale factor	11,51	m/s
Maximum energy yield	43800000	kWh
Capacity factor	0,510	-

Wind speed	Rayleigh distribution of yearly hours	Power curve	Energy yield kWh
0	0	0	0
1	131,2638535	0	0
2	256,6490587	0	0
3	370,7135714	0	0
4	468,8433849	23,7	11111,58822
5	547,5595989	143,2	78410,53456
6	604,7129288	369,2	223260,0133
7	639,5517254	746	476785,8113
8	652,6649246	1290,3	842133,5522
9	645,8155054	1907,7	1232022,24
10	621,6911003	2697,9	1677260,42
11	583,6050588	3596,5	2098935,594
12	535,1830388	4960,6	2654828,982
13	480,0673832	4927,1	2365340,004
14	421,6650992	4880,2	2057810,017
15	362,9565789	4911,9	1782806,42
16	306,3728029	4993	1529719,405
17	253,7400271	5065,5	1285320,108
18	206,2839408	5121,2	1056421,318
19	164,6805805	5104,4	840595,5552
20	129,139077	5051,6	652358,9616
21	99,50133132	4953,5	492879,8447
22	75,34548145	4897,7	369019,5645
23	56,08288189	4877,2	273527,4316
24	41,04163966	4938,1	202667,7208
25	29,53299319	5013,9	148075,4746
26	20,89959258	0	0
27	14,54682693	0	0
28	9,959684816	0	0
29	6,708287045	0	0
30	4,445329839	0	0
		Total	22351290,56

LC2: Spar-buoy

Variable	Value	Unit
Mean velocity	10,20	m/s
Nominal power	5000	kW
Scale factor	11,51	m/s
Maximum energy yield	43800000	kWh
Capacity factor	0,495	-

Wind speed	Rayleigh distribution of yearly hours	Power curve	Energy yield kWh
0	0	0	0
1	131,2638535	0	0
2	256,6490587	0	0
3	370,7135714	0	0
4	468,8433849	26	12189,92801
5	547,5595989	195,1	106828,8777
6	604,7129288	470	284215,0765
7	639,5517254	848	542020,0873
8	652,6649246	1284,5	838348,0956
9	645,8155054	1773,2	1145160,054
10	621,6911003	2448,1	1521961,983
11	583,6050588	3337,3	1947665,163
12	535,1830388	3951,5	2114775,778
13	480,0673832	4968,9	2385406,82
14	421,6650992	5039,4	2124939,101
15	362,9565789	5091,9	1848138,604
16	306,3728029	5104,4	1563849,335
17	253,7400271	5059,1	1283696,171
18	206,2839408	4985,6	1028449,215
19	164,6805805	4920,5	810310,7965
20	129,139077	4890,4	631541,7424
21	99,50133132	4923,1	489855,0042
22	75,34548145	4982,6	375416,3959
23	56,08288189	5061,6	283869,115
24	41,04163966	5104,4	209492,9455
25	29,53299319	5103,6	150724,584
26	20,89959258	0	0
27	14,54682693	0	0
28	9,959684816	0	0
29	6,708287045	0	0
30	4,445329839	0	0
		Total	21698854,87

LC3: Semi-submersible

Variable	Value	Unit
Mean velocity	10,20	m/s
Nominal power	5000	kW
Scale factor	11,51	m/s
Maximum energy yield	43800000	kWh
Capacity factor	0,505	-

Wind speed	Rayleigh distribution of yearly hours	Power curve	Energy yield kWh
0	0	0	0
1	131,2638535	0	0
2	256,6490587	0	0
3	370,7135714	0	0
4	468,8433849	105,1	49275,43975
5	547,5595989	207,1	113399,5929
6	604,7129288	357,2	216003,4581
7	639,5517254	578	369788,8076
8	652,6649246	918,9	599733,7992
9	645,8155054	1611,2	1040537,942
10	621,6911003	2392,7	1487520,296
11	583,6050588	3302,2	1927180,625
12	535,1830388	5182,5	2773586,098
13	480,0673832	5211,8	2502015,188
14	421,6650992	5294,3	2232421,534
15	362,9565789	5323	1932017,87
16	306,3728029	5300,2	1623837,13
17	253,7400271	5219,5	1324396,072
18	206,2839408	5103,2	1052708,207
19	164,6805805	4962,3	817194,4447
20	129,139077	4838,5	624839,4243
21	99,50133132	4745,5	472183,5678
22	75,34548145	4693,8	353656,6208
23	56,08288189	4686,3	262821,2094
24	41,04163966	4730,5	194147,4764
25	29,53299319	4812,7	142133,4363
26	20,89959258	0	0
27	14,54682693	0	0
28	9,959684816	0	0
29	6,708287045	0	0
30	4,445329839	0	0
		Total	22111398,24

LC3: Spar-buoy

Variable	Value	Unit
Mean velocity	10,20	m/s
Nominal power	5000	kW
Scale factor	11,51	m/s
Maximum energy yield	43800000	kWh
Capacity factor	0,492	-

Appendi

Wind speed	Rayleigh distribution of yearly hours	Power curve	Energy yield kWh
0	0	0	0
1	131,2638535	0	0
2	256,6490587	0	0
3	370,7135714	0	0
4	468,8433849	160,4	75202,47893
5	547,5595989	323,3	177026,0183
6	604,7129288	545,1	329629,0175
7	639,5517254	826	528461,5907
8	652,6649246	1178,1	768904,5476
9	645,8155054	1753,2	1132243,744
10	621,6911003	2397	1490193,568
11	583,6050588	3049,9	1779937,069
12	535,1830388	3744,4	2003939,37
13	480,0673832	4832,7	2320021,643
14	421,6650992	4922,9	2075815,117
15	362,9565789	5039,8	1829228,567
16	306,3728029	5145,7	1576502,532
17	253,7400271	5235,2	1328379,79
18	206,2839408	5270,3	1087178,253
19	164,6805805	5261	866384,5341
20	129,139077	5193,1	670632,141
21	99,50133132	5105,8	508033,8975
22	75,34548145	4997,7	376554,1126
23	56,08288189	4905,8	275131,402
24	41,04163966	4817,7	197726,3074
25	29,53299319	4775,2	141025,9491
26	20,89959258	0	0
27	14,54682693	0	0
28	9,959684816	0	0
29	6,708287045	0	0
30	4,445329839	0	0
		Total	21538151,65